

GPC-04-104
Revision 1
March 1983
GPC004.0104

DESIGN REPORT
FOR
RECIRCULATION SYSTEM
AND
RESIDUAL HEAT REMOVAL SYSTEM
WELD OVERLAY REPAIRS
AND FLAW EVALUATION
AT
E. I. HATCH NUCLEAR POWER PLANT
UNIT 1

Prepared for
Georgia Power Company

Prepared by
NUTECH Engineers, Inc.
San Jose, California

Prepared by:

J E Charnley

J. E. Charnley, P.E.
Project Engineer

Reviewed by:

P. E. Reeves

P. E. Reeves
Project Quality Assurance Engineer

Approved by:

P. C. Riccardella

P. C. Riccardella, P.E.
Senior Director

Issued by:

Norman Eng

N. Eng
Project Manager

Date: March 4, 1983

8305060055 830428
PDR ADDCK 05000321
P PDR

nutech
ENGINEERS

REVISION CONTROL SHEET

Design Report for Recirculation System
 TITLE: and Residual Heat Removal System Weld Overlay Repairs and Flaw Evaluation at Hatch 1
 REPORT NUMBER: GPC-04-104
 Revision 1

J. E. Charnley/Principal Engineer	<i>JEC</i>
P. C. Riccardella/Senior Director	<i>PCR</i>
Y. S. Wu/Consultant I	<i>YSW</i>
K. W. Benting/Consultant I	<i>KWB</i>
J. R. Taylor/Consultant II	<i>JRT</i>
T. Lem/Consultant I	<i>T.L</i>
R. D. Carignan/Principal Engineer	<i>RDC</i>
H. L. Gustin/Engineer	<i>H.L.G</i>
NAME / TITLE	INITIALS

PAGE(S)	REV	PREPARED BY / DATE	ACCURACY CHECK BY / DATE	CRITERIA CHECK BY / DATE	REMARKS
ii	0	<i>JEC 1/25/83</i>	<i>PCR 1/25/83</i>	<i>JRT 1/25/83</i>	
iii					
iv					
v					
vi					
vii					
viii					
ix					
x					
1					
2					
3					
4					
5					
6					
7					
8					
9					
10					
11					
12					
13					
14			<i>PCR 1-25-83</i>		
15			<i>PCR 1-25-83</i>		
16			<i>H.L.G 1-25-83</i>		
17			<i>H.L.G 1-25-83</i>		
18			<i>YSW 1-25-83</i>		
19					
20					
21					
22					

QEP 3-3.1.1
 REV 0

REVISION CONTROL SHEET

(CONTINUATION)

Design Report for
 TITLE: Recirculation System and Residual Heat Removal System Weld Overlay Repairs and Flaw Evaluation at Hatch 1
 REPORT NUMBER: GPC-04-104
 Revision 1

PAGE(S)	REV	PREPARED BY / DATE	ACCURACY CHECK BY / DATE	CRITERIA CHECK BY / DATE	REMARKS
23	0	JQC 1/25/83	KWB 1/25/83	<i>[Signature]</i>	
24			KWB 1/25/83		
25			YSW 1-25-83		
26					
27					
28					
29					
30					
31			RND 1-25-83		
32			RND 1-25-83		
33			YSW 1-25-83		
34					
35					
36					
37			TL 1/25/83		
38			YSW 1-25-83		
39					
40					
41					
42			JRT 1/25/83		
43			JRT 1/25/83		
44			JRD 1-25-83		
45					
46					
47					
48			RND 1-25-83		
49			HLD 1-25-83		
50			HLD 1-25-83		
51			YSW 1-25-83		
52					
53					
54					
55			KWB 1/25/83		
56			YSW 1-25-83		
57					
58					
59			RND 1-25-83		
60			YSW 1-25-83		
61					
62			TL 1/25/83		
63					
64					
65			YSW 1-25-83		
66					
67			JRT 1/25/83		
68			<i>[Signature]</i> 1/25/83		
69					
70					

REVISION CONTROL SHEET

Design Report for (CONTINUATION)
 TITLE: Recirculation System and Residual Heat Removal System Weld Overlay Repairs and Flaw Evaluation at Hatch 1
 REPORT NUMBER: GPC-04-104
 Revision 1

PAGE(S)	REV	PREPARED BY / DATE	ACCURACY CHECK BY / DATE	CRITERIA CHECK BY / DATE	REMARKS
71	0	JRC 1/25/83	RLC 1/25/83	RLC 1/25/83	
72					
73					
74					
75					
76					
77					
78					
79					
80					
81					
82					
83					
84					
85	1	JRC 3/2/83	HRS 3/3/83	RLC 3/3/83	
3					
5					
6					
7					
16			HRS 3/3/83		
19			YSW 3/2/83		
21					
22			YSW 3/2/83		
29					
30					
35					
36					
38			RLC 3/3/83		
41			YSW 3/2/83		
48			HRS 3/3/83		
55			YSW 3/2/83		
81			YSW 3/2/83		
87			RLC 3/3/83		
88					
89					
90					

CERTIFICATION BY REGISTERED PROFESSIONAL ENGINEER

I hereby certify that this document and the calculations contained herein were prepared under my direct supervision, reviewed by me, and to the best of my knowledge are correct and complete. I am a duly Registered Professional Engineer under the laws of the State of California and am competent to review this document.

Certified by:

J E Charnley

J. E. Charnley



Professional Engineer
State of California
Registration No. 16340

Date 4 March 1983

TABLE OF CONTENTS

	<u>Page</u>
LIST OF TABLES	vii
LIST OF FIGURES	viii
1.0 INTRODUCTION	1
2.0 REPAIR DESCRIPTION	4
3.0 EVALUATION CRITERIA	8
3.1 Weld Overlay Evaluation	8
3.1.1 Strength Evaluation	9
3.1.2 Fatigue Evaluation	9
3.1.3 Crack Growth Evaluation	10
3.2 Flaw Evaluation	11
4.0 LOADS	12
4.1 Mechanical and Internal Pressure Loads	12
4.2 Thermal Loads	12
5.0 EVALUATION METHODS AND RESULTS	14
5.1 End Cap Evaluation	14
5.1.1 Code Stress Analysis	15
5.1.2 Fracture Mechanics Evaluation	17
5.2 Elbow Evaluation	24
5.2.1 Code Stress Analysis	24
5.2.2 Fracture Mechanics Evaluation	26
5.3 Pipe-to-Pipe Evaluation	31
5.3.1 Code Stress Analysis	32
5.3.2 Fracture Mechanics Evaluation	33
5.4 Sweepolet Evaluation	37
5.4.1 Code Stress Analysis	38
5.4.2 Fracture Mechanics Evaluation	39
5.5 Effect on Recirculation and RHR Systems	43

TABLE OF CONTENTS
(Continued)

	<u>Page</u>
6.0 LEAK-BEFORE-BREAK	69
6.1 Net Section Collapse	69
6.2 Tearing Modulus Analysis	70
6.3 Leak Versus Break Flaw Configuration	71
6.4 Axial Cracks	72
6.5 Multiple Cracks	73
6.6 Crack Detection Capability	73
6.7 Non-Destructive Examination	74
6.8 Leakage Detection	75
6.9 Historical Experience	76
7.0 SUMMARY AND CONCLUSIONS	82
8.0 REFERENCES	84
9.0 ENGINEERING CHANGES	87

LIST OF TABLES

<u>Number</u>	<u>Title</u>	<u>Page</u>
5.1	Thermal Stress Results	45
5.2	End Cap Code Stress Results	46
5.3	Elbow Code Stress Results	47
5.4	Pipe-to-Pipe Code Stress Results	48
6.1	Effect of Pipe Size on the Ratio of the Crack Length for 5 GPM Leak Rate and the Critical Crack Length (Assumed Stress $\sigma = (S_m)/2$)	77

LIST OF FIGURES

<u>Number</u>	<u>Title</u>	<u>Page</u>
1.1	Conceptual Drawing of Recirculation and RHR Systems	3
2.1	Schematic of End Cap Weld Overlay	5
2.2	Schematic of Elbow-to-Pipe Weld Overlay	6
2.3	Schematic of Pipe-to-Pipe Weld Overlay	7
5.1	End Cap Finite Element Model	49
5.2	Weld Overlay Thermal Model	50
5.3	Thermal Transients	51
5.4	Axial Crack Growth Residual Stress	52
5.5	Typical IGSCC Crack Growth Data (Weld Sensitized 304SS in BWR Environment)	53
5.6	End Cap Axial Crack Growth	54
5.7	End Cap Tearing Modulus	55
5.8	Elbow Finite Element Model	56
5.9	Circumferential Crack Growth Residual Stress	57
5.10	Elbow Circumferential Crack Growth	58
5.11	Elbow Tearing Modulus	59
5.12	Pipe-to-Pipe Finite Element Model	60
5.13	Pipe-to-Pipe Axial Crack Growth	61
5.14	Pipe-to-Pipe Tearing Modulus	62
5.15	Sweepolet Crack Geometry	63
5.16	Sweepolet Finite Element Model (Outside)	64
5.17	Sweepolet Finite Element Model (Inside)	65
5.18	Sweepolet Crack Growth	66

LIST OF FIGURES
(Continued)

<u>Number</u>	<u>Title</u>	<u>Page</u>
5.19	Sweepolet Tearing Modulus	67
5.20	Piping Model	68
6.1	Typical Result of Net Section Collapse Analysis of Cracked Stainless Steel Pipe	78
6.2	Stability Analysis for BWR Recirculation System (Stainless Steel)	79
6.3	Summary of Leak-Before-Break Assessment of BWR Recirculation System	80
6.4	Typical Pipe Crack Failure Locus for Combined Through-Wall Plus 360° Part-Through Crack	81
9.1	Sketch of BR-13 Overlay Toe Crack	88
9.2	Sketch of Revised BR-13 Overlay	89
9.3	Revised Pipe-to-Pipe Finite Element Model	90

This report summarizes evaluations performed by NUTECH to assess weld overlay repairs and unrepaired flaws in the Recirculation and Residual Heat Removal (RHR) Systems at Georgia Power Company's Edwin I Hatch Nuclear Plant Unit 1. Weld overlay repairs have been applied to address leakage and additional ultrasonic (UT) examination results believed to be indicative of intergranular stress corrosion cracking (IGSCC) in the vicinity of the welds. The purpose of each overlay is to arrest any further propagation of the cracking, and to restore original design safety margins to the weld. The unrepaired welds which had UT examination indications have been shown by analysis to continue to have the original design safety margins.

The required design life of each weld overlay repair is at least two fuel cycles. The amount that the actual design life exceeds two fuel cycles will be established by a combination of future analysis and testing.

Leakage was observed during overlay welding adjacent to one end cap-to-manifold weld and in addition, crack indications have been detected adjacent to three end

cap-to-manifold welds, one elbow-to-pipe weld, one pipe-to-pipe weld and one sweepolet-to-manifold weld. All of these welds except the sweepolet-to-manifold weld were repaired with weld overlay designs evaluated in this report. The analysis of the unrepaired sweepolet weld is also contained herein.

Figure 1.1 shows the end caps, elbow, sweepolet and pipe-to-pipe welds in relation to the reactor pressure vessel and other portions of the recirculation and RHR systems. All of the existing material is type 304 stainless steel.

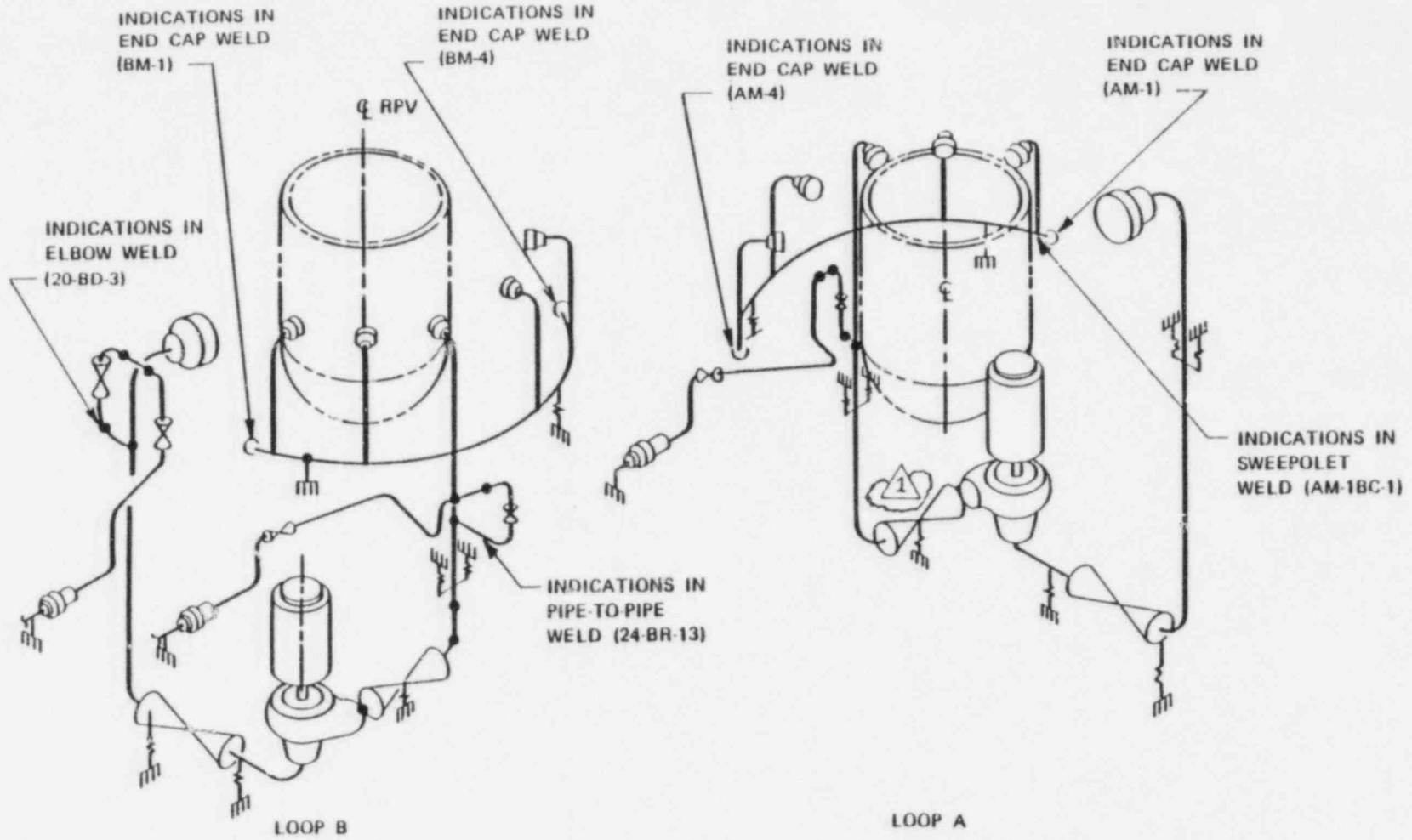


Figure 1.1
CONCEPTUAL DRAWING OF RECIRCULATION AND RHR SYSTEMS

REPAIR DESCRIPTION

The through-wall cracks and other indications around and to both sides of the existing end cap, pipe-to-pipe and elbow weld heat-affected zones have been repaired by establishing additional "cast-in-place" pipe wall thickness from weld metal deposited 360 degrees around and to either side of the existing weld, as shown in Figures 2.1, 2.2, and 2.3. The weld deposited band over the cracks will provide wall thickness equal to that required to provide the original design safety margins. In addition, the weld metal deposition will produce a favorable compressive residual stress pattern. The deposited weld metal will be type 308L, which is resistant to propagation of IGSCC cracks.

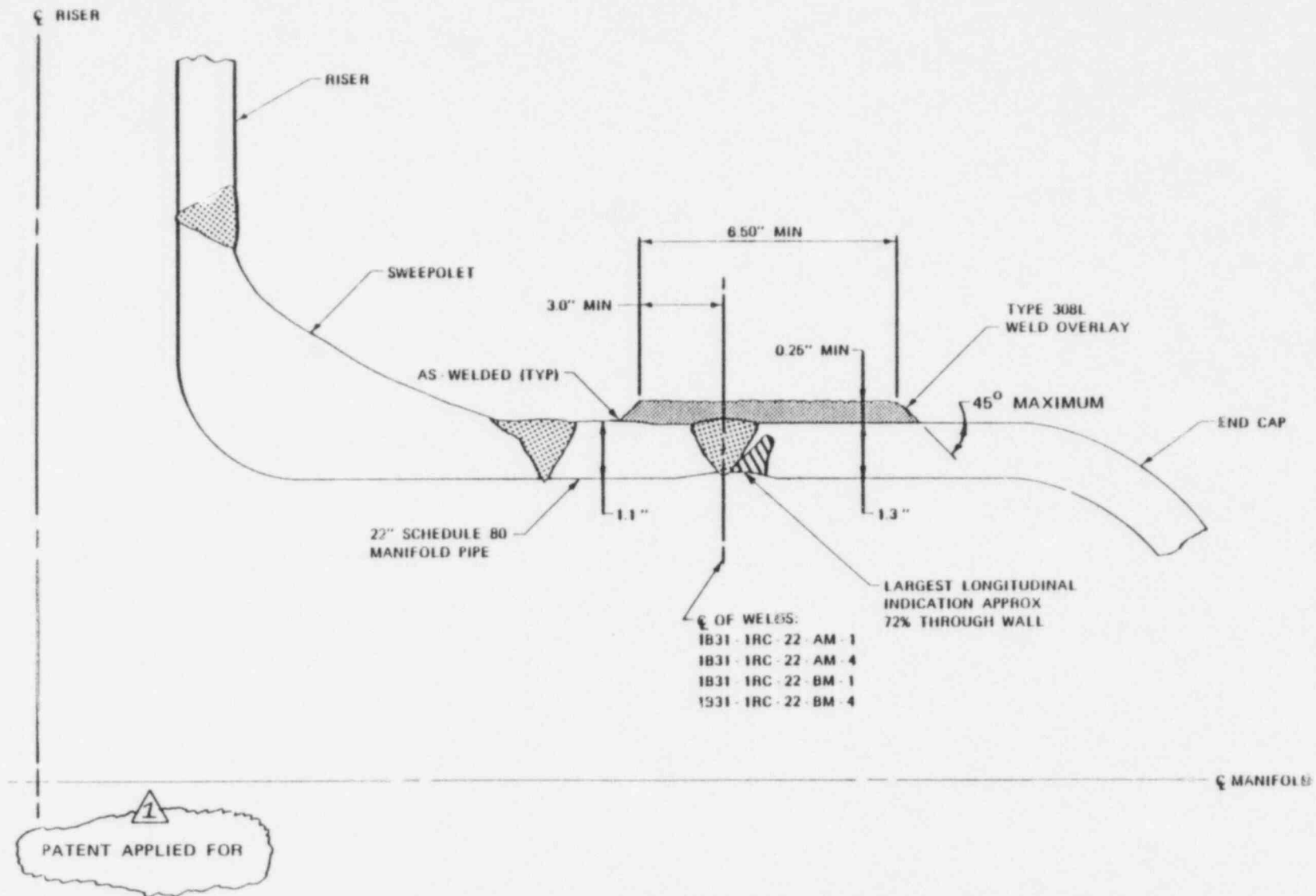
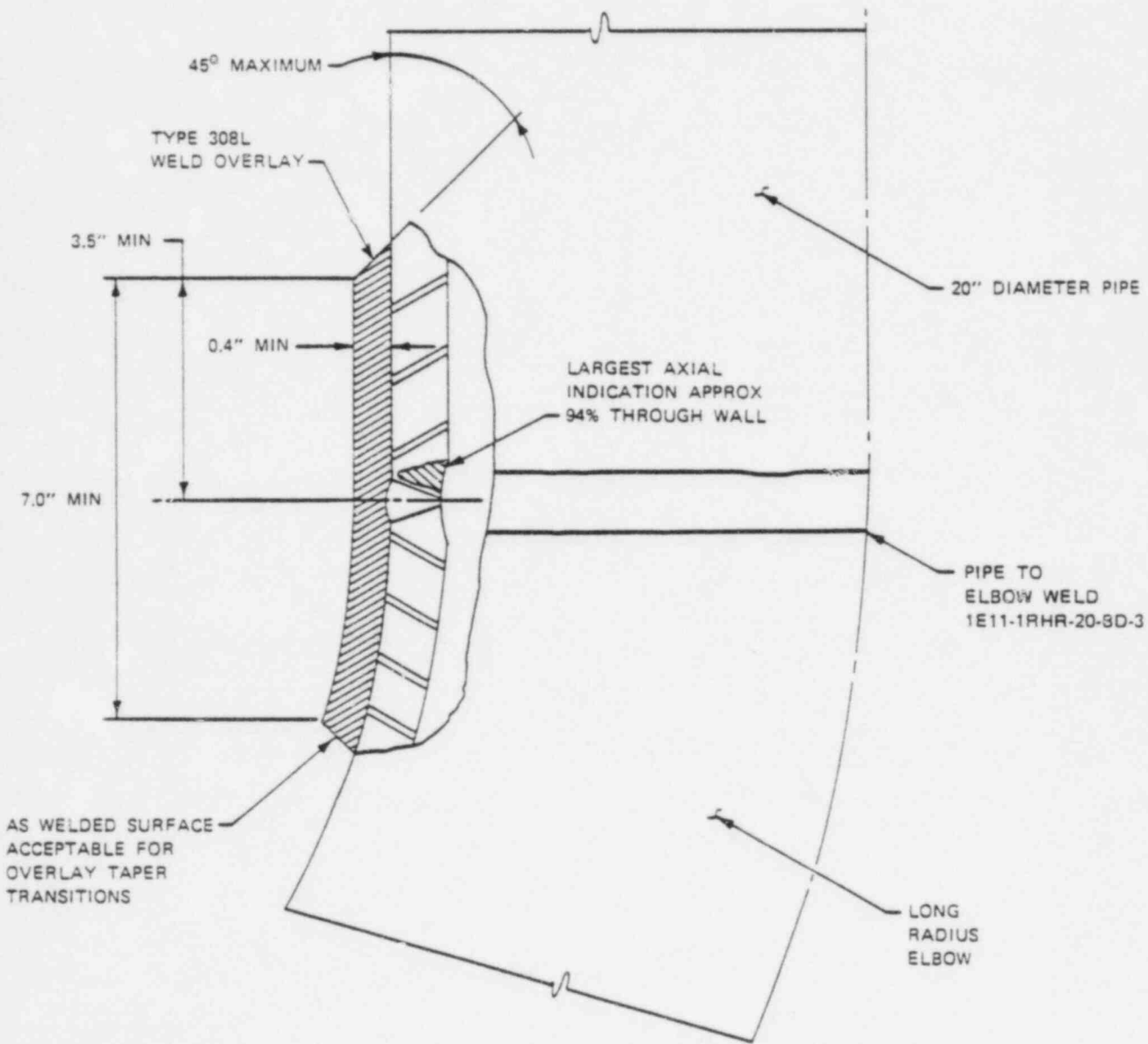


Figure 2.1
SCHEMATIC OF END CAP WELD OVERLAY



1
PATENT APPLIED FOR

Figure 2.2
SCHEMATIC OF ELBOW TO PIPE WELD OVERLAY

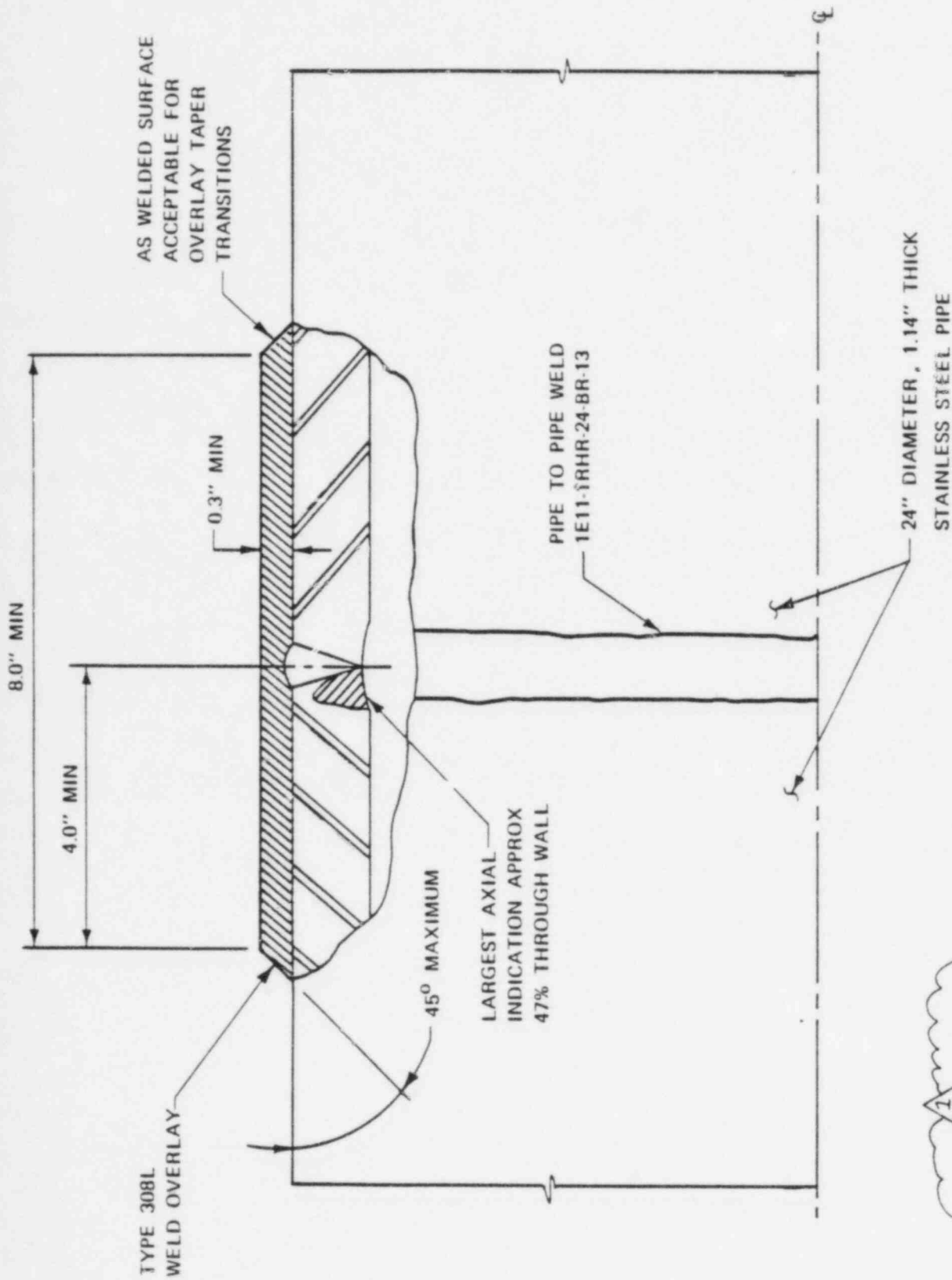


Figure 2.3
SCHEMATIC OF PIPE-TO-PIPE WELD OVERLAY

3.0 EVALUATION CRITERIA

3.1 Weld Overlay Evaluation

This section describes the criteria that are applied in this report to evaluate the acceptability of the weld overlay repairs described in Section 2.0. Because of the nature of these repairs, the geometric configuration is not directly covered by Section III of the ASME Boiler and Pressure Vessel Code, which is intended for new construction. However, materials, fabrication procedures, and Quality Assurance requirements are in accordance with applicable sections of this Construction Code, and the intent of the design criteria described below is to demonstrate equivalent margins of safety for strength and fatigue considerations as provided in the ASME Section III Design Rules. In addition, because of the IGSCC conditions that led to the need for repairs, IGSCC resistant materials have been selected for the weld overlay repairs. As a further means of ensuring structural adequacy, criteria are also provided below for fracture mechanics evaluation of the repairs.

3.1.1 Strength Evaluation

Adequacy of the strength of the weld overlay repairs with respect to applied mechanical loads is demonstrated with the following criteria:

1. An ASME Boiler and Pressure Vessel Code Section III, Class 1 (Reference 1) analysis of the weld overlay repairs was performed.
2. The ultimate load capacity of the repairs was calculated with a tearing modulus analysis. The ratio between failure load and applied loads was required to be greater than that required by Reference 1.

3.1.2 Fatigue Evaluation

The stress values obtained from the above strength evaluation were combined with thermal and other secondary stress conditions to demonstrate adequate fatigue resistance for the design life of each repair. The criteria for fatigue evaluation include:

1. The maximum range of primary plus secondary stress was compared to the secondary stress limits of Reference 1.

2. The peak alternating stress intensity, including all primary and secondary stress terms, and a fatigue strength reduction factor of 5.0 to account for the existing crack, was evaluated using conventional fatigue analysis techniques. The total fatigue usage factor, defined as the sum of the ratios of applied number of cycles to allowable number of cycles at each stress level, must be less than 1.0 for the design life of each repair. Allowable number of cycles was determined from the stainless steel fatigue curve of Reference 1.

3.1.3 Crack Growth Evaluation

Crack growth due to both fatigue (cyclic stress) and IGSCC (steady state stress) was calculated. The allowable crack depth was established based on net section limit load for each cracked and repaired weld (Reference 2). The design life of each repair was

established as the minimum of either the predicted time for the observed crack to grow to the allowable crack depth or five years.

3.2 Flaw Evaluation

Crack growth due to both fatigue (cyclic stress) and IGSCC (steady state stress) was calculated. The allowable crack depth was established based on the net section limit load for the cracked sweepolet weld (Reference 2).

The life of the sweepolet weld with the observed flaw was established as the time for the flaw to grow to the allowable crack depth.

4.0 LOADS

The loads considered in the evaluation of the sweepolet, end cap, pipe-to-pipe and elbow welds consist of mechanical loads, internal pressure, differential thermal expansion loads, and welding residual stresses. The mechanical loads and internal pressures used in the analysis are described in Section 4.1, and an explanation of the thermal transient conditions which cause differential thermal expansion loads is presented in Section 4.2. Welding residual stresses are considered in the crack growth analyses and are described in Sections 5.1.2.2 and 5.2.2.2.

4.1 Mechanical and Internal Pressure Loads

The design pressure of 1325 psi for the Recirculation and RHR Systems was obtained from Reference 3. The dead weight and seismic loads applied to each weld were obtained from Reference 4.

4.2 Thermal Loads

The thermal expansion loads for each weld were also obtained from Reference 4 and applied to the weld

overlay repairs. Reference 3 defines several types of transients that the Recirculation and RHR Systems are designed for. These transients were conservatively grouped into three composite transients. The first composite transient is a startup/shutdown transient with a heatup or cool down rate of 100°F per hour. The second composite transient consists of a 50°F step temperature with no change in pressure. The third composite transient is an emergency event with a 416°F step temperature change and a pressure change of 1325 psi. In the five year overlay design life, there are 38 startup/shutdown cycles, 25 small temperature change cycles, and 1 emergency cycle.

5.0 EVALUATION METHODS AND RESULTS

The evaluation of the weld overlay repairs and the unrepaired sweeplet weld consists of a code stress analysis per Section III (Reference 1) and a fracture mechanics evaluation per Section XI (Reference 5).

5.1 End Cap Evaluation

The four end cap welds with ultrasonic indications are:

- 1) 1B31-1RC-22-AM-1 with maximum depth of 63% of wall
- 2) 1B31-1RC-22-AM-4 with maximum depth of 72% of wall
- 3) 1B31-1RC-22-BM-1 with maximum depth of 64% of wall
- 4) 1B31-1RC-22-BM-4 with maximum depth of 67% of wall

All indications are axial, with a length of approximately 1/2".

During the installation of the weld overlays, porosity appeared on the exterior surface of the AM-4, BM-4, and BM-1 end cap welds. The locations of the porosity were recorded and the weld overlays completed. The porosity was then repaired by grinding back to base metal and filling the cavity with shielded metal arc welding.

5.1.1 Code Stress Analysis

The weld overlaid regions were assumed to be axisymmetric. That is, a 75% through-wall axial crack was conservatively assumed to be 360 degrees around the pipe and 1/2 inch long on the end cap side of the weld. It is judged that the assumed crack geometry conservatively envelopes all observed cracks in the end cap welds. In addition, all analyses were conservatively performed using a weld overlay thickness of 0.25 inch which is 10 percent smaller than the actual minimum average thickness of 0.275 inch. A finite element model of the cracked and weld overlaid region was developed using the ANSYS (Reference 6) computer program. Figure 5.1 shows the model.

Based on Reference 4, the applied thermal, weight and seismic moments on these welds are negligible. The pressure stress for a design pressure of 1325 psi was calculated with this model. The weld overlay thermal model was also taken to be axisymmetrical (Figure 5.2). The exterior boundary was assumed to be insulated. The temperature distribution in the weld overlay subject to the thermal transients defined in Section 4.2 can be readily calculated using Charts 16

and 23 of Reference 7. The maximum through-wall temperature difference was determined to be less than 2°F for the normal startup cycle, 40°F for the small temperature cycle and 329°F for the emergency transient.

The maximum thermal stress for use in the fatigue crack growth analysis was calculated as follows: (Reference 1)

$$s = \frac{Ea \Delta T_1}{2(1-\nu)} + \frac{Ea \Delta T_2}{1-\nu}$$

Where:

E = 28.3 x 10⁶ psi (Young's Modulus)

a = 9.11 x 10⁻⁶ °F⁻¹

(Coefficient of Thermal Expansion)

ΔT_1 = Equivalent Linear Temperature Difference

ΔT_2 = Peak Temperature Difference

The values of ΔT_1 , ΔT_2 , and s are given in Table 5.1 for all three thermal transients.

The results of a code stress analysis per Reference 1 are given in Table 5.2. The allowable stress values for

Reference 1 are also given. The weld overlay repair satisfies the Reference 1 requirements.

A conservative fatigue analysis per Reference 1 was performed. In addition to the stress intensification factors required per Reference 1, an additional fatigue strength reduction factor of 5.0 was applied due to the crack. The fatigue usage factor was then calculated assuming 38 startups, 25 small temperature change cycles and one emergency cycle every five years. The results are summarized in Table 5.2.

5.1.2 Fracture Mechanics Evaluation

Three types of fracture mechanics evaluations were performed. The allowable crack depth was calculated based on Reference 2. Crack growth due to both fatigue and IGSCC was calculated using the NUTECH computer program NUTCRAK (Reference 8) with material constants and methodology from References 9 and 10. Finally, the ultimate margin to failure for a crack assumed to propagate all the way through the original pipe material to the weld overlay was calculated per References 11 and 12.

5.1.2.1 Allowable Crack Depth

The allowable depth for a 1/2 inch long axial crack was determined using Reference 2. The dimensions of the repaired pipe were used. Thus, the ratio of applied primary stress to Code allowable stress (S_m) was calculated in the following manner:

$$\text{Stress Ratio} = \frac{PR/t}{S_m}$$

- P = 1325 psi (Design Pressure)
- R = 11.20 inches (Outside Radius of Pipe)
- t = 1.24 inches (Nominal Pipe Thickness)
- S_m = 16,800 psi (Reference 1)

Substitution yields:

$$\text{Stress Ratio} = .71$$

The nondimensional crack length (\bar{l}) was calculated in the following manner:

$$\bar{a} = \frac{a_f}{(rt)^{1/2}}$$

$$\begin{aligned} a_f &= 1/2 \text{ inch} \\ r &= 10.58 \text{ inches (mean radius of pipe)} \\ t &= 1.24 \text{ inches} \end{aligned}$$

Substitution yields:

Nondimensional Length = .14

Thus per Table IWB-3642-1 of Reference 2, the allowable crack depth is 75 percent of the wall thickness.

5.1.2.2 Crack Growth

The existing cracks could grow due to both fatigue and stress corrosion. Fatigue crack growth due to the three types of thermal transients defined in Section 4.2 was calculated using the material properties from Reference 9. The fatigue cycles considered are shown in Figure 5.3. The fatigue crack growth for 5 years was calculated to be less than 0.01 inch.

IGSCC growth depends on the total steady state stress. The major contributor to the steady state stress is the weld residual stress. The residual stress due to the original butt weld was conservatively chosen to be a worst case with through-wall bending stress of 30,000 psi with tension on the inside surface. The weld residual stress due to the overlay was based on preliminary results of a weld overlay optimization study sponsored by the Electric Power Research Institute (EPRI). The residual stress due to a weld overlay depends on the size of the overlay and on whether the direction of interest is hoop or axial. Figure 5.4 shows the hoop direction (axial cracks) residual stress for the worst case without an overlay and for a 1/4 thickness overlay plus the worst case original residual stress.

The IGSCC crack growth rate as a function of applied stress intensity factor is shown in Figure 5.5. The upper bound crack growth law of Figure 5.5 was used for all analyses:

$$\frac{da}{dT} = 4.116 \times 10^{-12} K^{4.615}$$

where:

da = differential crack size
dT = differential time
K = applied stress intensity factor

Crack growth as a function of time was calculated by conservatively assuming an infinitely long crack and using the NUTECH computer code NUTCRAK (Reference 8). The results are shown in Figure 5.6 for an initial crack depth of 0.75 inch ($a/t = \frac{0.75}{1.24} = 0.60$). Figure 5.6 shows that a 0.75 inch deep crack will grow to a depth of approximately 0.85 inch in five years when the beneficial residual stress due to the weld overlay is considered.

The length of axial cracks is limited by the width of the original butt weld heat affected zone. The weld overlay technique is designed to minimize additional sensitization by using low weld heat input during the first two layers of weld. Thus the potential for additional crack growth in the axial direction is minimized. The maximum axial growth of axial cracks underneath a weld overlay was determined in Reference 13

to be less than 0.01 inch in five years. This axial growth is judged to be insignificant.

The worst case for an end cap overlay occurs for the end caps that have a crack completely through the original pipe. The crack will not propagate into the overlay weld material due to IGSCC but will grow approximately 0.01 inch due to fatigue in 5 years. Thus, the worst case axial crack depth is 1.01 inch which is 79 percent of as-built total wall thickness. Although the crack depth after 5 years exceeds the Reference 2 allowable depth by 4 percent of wall thickness, the weld overlay design is judged to be acceptable for the following reason. The allowable crack depths in Reference 2 were not allowed to exceed 75% of the wall thickness even though net section collapse analysis would permit much larger cracks for very short crack lengths. This truncation is somewhat artificial and could be eliminated for short, almost through-wall cracks, if leaks are prevented by a weld overlay. Elimination of the truncation results is an allowable depth in excess of 79 percent. Thus, the overlay design is acceptable for 5 years.

5.1.2.3 Tearing Modulus

The largest size to which the existing crack could reasonably be expected to grow was postulated to be a one inch radius flaw. This assumes growth of the crack in the radial direction completely through the original pipe material to the overlay. After such propagation, the assumed crack would be completely surrounded by IGSCC resistant material: the weld between end cap and manifold, the weld overlay, and the end cap and manifold. A tearing modulus evaluation was then performed for this postulated crack. The only applied load was pressure.

The evaluation was performed using the methodology of Reference 11 with material properties from Reference 12.

The postulated flaw and the results are shown in Figure 5.7. The upper dotted line represents the inherent material resistance to unstable fracture in terms of J-integral and Tearing Modulus, T . The line originating at the origin represents the applied loading. Increasing pressure results in applied J-T combination moving up this line, and unstable fracture

is predicted at the intersection of this applied loading line with the material resistance line.

Figure 5.7 shows that the predicted burst pressure is in excess of 5500 psig. Thus, there is a safety factor on design pressure of at least 4, which is well in excess of the safety factor inherent in the ASME Code, even in the presence of this worst case assumed crack.

5.2 Elbow Evaluation

The largest measured ultrasonic indications in elbow-to-pipe weld number 1E11-1RHR-20-BD-3 are an axial crack of depth 94% of wall and length of 3/8 inch, and a circumferential crack of length 1-1/2 inches and depth approximately 33% of wall.

5.2.1 Code Stress Analysis

A finite element model of the cracked and weld overlaid region was developed using the ANSYS (Reference 6) computer program. Figure 5.8 shows the model. This figure also shows the material that was removed to represent the cracks.

Based on Reference 4, the applied moments on these welds are:

Weight + OBE Seismic = 743,100 inch-pounds

Weight + Steady State Thermal = 636,100 inch-pounds

SSE loads are not limiting for the elbow.

The thermal analysis was performed in the same manner as for the end cap (Section 5.1.1), with appropriate dimensional changes.

The results of a code stress analysis per Reference 1 are given in Table 5.3. The allowable stress values for Reference 1 are also given. The weld overlay repair satisfies the Reference 1 requirements.

A conservative fatigue analysis per Reference 1 was performed. A fatigue strength reduction factor of 5.0 was applied due to the crack. The fatigue usage factor was then calculated assuming 38 startups, 25 small temperature change cycles and one emergency cycle every five years. The results are summarized in Table 5.3.

5.2.2 Fracture Mechanics Evaluation

Three types of fracture mechanics evaluations were performed. The allowable crack depth was calculated based on Reference 2. Crack growth due to both fatigue and IGSCC was calculated using the NUTECH computer program NUTCRAK (Reference 8) with material constants and methodology from References 9 and 10. Finally, the ultimate margin to failure for a crack assumed to propagate all the way through the original pipe material to the weld overlay was calculated per References 11 and 12.

5.2.2.1 Allowable Crack Depth

The allowable depth for a 3/8 inch long axial crack was determined using Reference 2. The dimensions of the repaired elbow were used. Thus, the ratio of applied primary stress to Code allowable stress (S_m) was calculated in the following manner:

$$\text{Stress Ratio} = \frac{PR/t}{S_m}$$

P = 1325 psi
R = 10.50 inches (Outside Radius of Overlay)
t = 1.16 inches (Overlaid Pipe Thickness)
S_m = 16,800 psi

Stress Ratio = .71

The nondimensional crack length (\bar{l}) was calculated in the following manner:

$$\bar{l} = \frac{l_f}{(rt)^{1/2}}$$

l_f = .375 inch (Crack Length)
r = 9.87 inches (Mean Radius of Pipe)
t = 1.24 inches
 \bar{l} = .11

Thus, per Table IWB-3642-1 of Reference 2, the allowable crack depth is 75 percent of the overlaid wall thickness or a depth of 0.87 inch. Emergency and faulted conditions are not limiting.

The allowable depth of a 1-1/2 inch long circumferential crack was also determined using Reference 2. From Table 5.3, the primary stress at the crack location is 16,200 psi. Thus the stress ratio was calculated in the following manner:

$$\text{Stress Ratio} = \frac{P_m + P_b}{S_m} = \frac{16,200}{16,800} = .96$$

The nondimensional crack length was calculated in the following manner:

$$\bar{a} = \frac{a_f}{2\pi R} = \frac{1.5}{2\pi(10.5)} = .02$$

Thus based on Table IWB-3641-1 of Reference 2, the allowable crack depth is 75 percent of the wall thickness. Emergency and faulted conditions are not limiting.

5.2.2.2 Crack Growth

Crack growth was calculated in a manner similar to Section 5.1.2.2, except: 1) the residual stress due to the weld overlay was changed to represent a one-half thickness overlay; 2) the axial residual stress was used for the circumferential crack.

The axial crack which is essentially through-wall will grow into the IGSCC resistant weld overlay only due to fatigue. The fatigue crack growth for five years of the thermal cycles shown in Figure 5.3 is less than 0.01 inch. Thus, the axial crack depth after five years would be 0.77 inch which is 66 percent of overlaid wall thickness, which is less than the allowable of 75 percent.

Based on Reference 13, the axial growth of the axial crack will be less than 0.01 inch in five years.

The circumferential crack will grow due to both fatigue and IGSCC. The fatigue crack growth due to five years of the cycles shown on Figure 5.3 is less than 0.01 inch. The IGSCC crack growth was calculated using the upper bound growth curve shown in Figure 5.5 and the

residual stress curve shown in Figure 5.9. Crack depth as a function of time is shown in Figure 5.10. Thus, the circumferential crack depth after five years is approximately 0.26 inch which is 23 percent of the overlaid wall thickness which is less than the allowable of 75 percent. Thus, both the worst case axial crack and the worst case circumferential crack will not grow to an unacceptable size within the next 5 years.

5.2.2.3 Tearing Modulus

The largest size to which the existing axial crack could reasonably be expected to grow was postulated to be a 0.80 inch radius flaw. This assumes growth of the crack in the radial direction completely through the original pipe material to the overlay. After such propagation, the assumed crack would be completely surrounded by IGSCC resistant material: the weld between elbow and pipe, the weld overlay, and the elbow and pipe. A tearing modulus evaluation was then performed for this postulated crack. The normal operating loads of pressure, weight and thermal expansion were applied.

The evaluation was performed using the methodology of Reference 11 with material properties from Reference 12.

The postulated flaw and the results are shown in Figure 5.11. The upper dotted line represents the inherent material resistance to unstable fracture in terms of J-integral and Tearing Modulus, T. The line originating at the origin represents the applied loading. Increasing load results in applied J-T combinations moving up this line, and unstable fracture is predicted at the intersection of this applied loading line with the material resistance line.

Figure 5.11 shows that the predicted failure load is in excess of 3 times the normal operating loads. Thus, there is a safety factor on normal operating loads of at least 3, which is in excess of the safety factor inherent in the ASME Code, even in the presence of this worst case assumed crack.

5.3 Pipe-to-Pipe Evaluation

The pipe-to-pipe weld number 1E11-1RHR-24-BR-13 was determined by ultrasonic examination to have axial crack indications. The largest axial crack is approximately one-half inch long with a depth of approximately 47% of the wall thickness.

5.3.1 Code Stress Analysis

The weld overlaid regions were assumed to be axisymmetric. That is, a 47% through-wall axial crack was conservatively assumed to be 360 degrees around the pipe and 1/2 inch long centered on the weld. Thus, the assumed crack geometry conservatively envelopes all observed cracks in the pipe-to-pipe weld. In addition, all analyses were conservatively performed using a weld overlay thickness of 0.30 inch which is 25 percent smaller than the actual thickness of 0.375 inch. A finite element model of the cracked and weld overlaid region was developed using the ANSYS (Reference 6) computer program. Figure 5.12 shows the model.

Based on Reference 4, the applied thermal, weight and seismic moments on this weld are:

Weight + OBE Seismic = 1,113,000 inch-pounds

Weight + Steady State Thermal = 1,626,000 inch-pounds

SSE is not limiting for this weld. The thermal analysis was performed in the same manner as for the end cap

(Section 5.1.1), with appropriate dimensional changes. The results of a code stress analysis per Reference 1 are given in Table 5.4. The allowable stress values for Reference 1 are also given. The weld overlay repair satisfies the Reference 1 requirements.

A conservative fatigue analysis per Reference 1 was performed. An additional fatigue strength reduction factor of 5.0 was applied due to the crack. The fatigue usage factor was then calculated with the thermal transients shown in Figure 5.3. The results are summarized in Table 5.4.

5.3.2 Fracture Mechanics Evaluation

Three types of fracture mechanics evaluations were performed. The allowable crack depth was calculated based on Reference 2. Crack growth due to both fatigue and IGSCC was calculated using the NUTECH computer program NUTCRAK (Reference 8) with material constants and methodology from References 9 and 10. Finally, the ultimate margin to failure for a crack assumed to propagate all the way through the original pipe material to the weld overlay was calculated per References 11 and 12.

5.3.2.1 Allowable Crack Depth

The allowable depth for a 1/2 inch long axial crack was determined using Reference 2. The dimensions of the repaired pipe were used. Thus, the ratio of applied primary stress to Code allowable stress (S_m) was calculated in the following manner:

$$\text{Stress ratio} = \frac{PR/t}{S_m}$$

- P = 1325 psi (Design Pressure)
- R = 12.30 inches (Outside Radius of Overlay)
- t = 1.44 inches (Overlaid Pipe Thickness)
- S_m = 16,800 psi (Reference 1)

Substitution yields:

$$\text{Stress ratio} = .67$$

The nondimensional crack length (\bar{l}) was calculated in the following manner:

$$\bar{l} = \frac{l_F}{(rt)^{1/2}}$$

$$\begin{aligned} l_F &= 1/2 \text{ inch} \\ r &= 11.58 \text{ inches (Mean Radius of Pipe)} \\ t &= 1.44 \text{ inches} \end{aligned}$$

Substitution yields:

Nondimensional Length = .12

Thus per Table IWB-3642-1 of Reference 2, the allowable crack depth is 75 percent of the wall thickness.

Emergency and faulted conditions are not limiting.

5.3.2.2 Crack Growth

Crack growth was calculated in a manner similar to Section 5.1.2.2. The fatigue crack growth for five years of the cycle shown in Figure 5.3 is less than 0.01 inch. The IGSCC crack growth calculated with the upper bound growth law and an infinite crack length is shown in Figure 5.13. Thus, the axial cracks in the pipe-to-

pipe weld will not grow to an unacceptable size in the next 5 years.

Based on Reference 13, the axial growth of the axial crack will be less than 0.01 inch in five years.

5.3.2.3 Tearing Modulus

The largest size to which the existing crack could reasonably be expected to grow was postulated to be a 1.14 inch radius flaw. This assumes growth of the crack in the radial direction completely through the original pipe material to the overlay. After such propagation, the assumed crack would be completely surrounded by IGSCC resistant material: the pipe-to-pipe weld, the weld overlay, and the annealed piping. A tearing modulus evaluation was then performed for this postulated crack. The applied loads were pressure, seismic, steady state thermal and weight.

The evaluation was performed using the methodology of Reference 11 with material properties from Reference 12.

The postulated flaw and the results are shown in Figure 5.14. The upper dotted line represents the inherent

material resistance to unstable fracture in terms of J-integral and Tearing Modulus, T. The line originating at the origin represents the applied loading.

Increasing load results in applied J-T combinations moving up this line, and unstable fracture is predicted at the intersection of this applied loading line with the material resistance line.

Figure 5.14 shows that the predicted failure load is in excess of 4 times the normal loads. Thus, there is a safety factor on normal operating loads of at least 4, which is well in excess of the safety factor inherent in the ASME Code, even in the presence of this worst case assumed crack.

5.4 Sweepolet Evaluation

Seven small ultrasonic indications were found in the weld between a sweepolet and the 22 inch manifold (weld number 1B31-1RC-22AM-1BC-1). All the indications are transverse to the weld. The largest indication is approximately 1/2 inch long with a depth of approximately 12% of the wall. Figure 5.15 shows the approximate location of the indications.

5.4.1 Code Stress Analysis

Due to the three dimensional geometry of the sweepolet and the difficulty of performing a repair, a three-dimensional finite element model was developed using ANSYS (Reference 6). The geometry is symmetric about two perpendicular axes. Thus the sweepolet was represented with a 90° model as shown on Figures 5.16 and 5.17. The applied loads are not all symmetric about both axes. However, the majority of the stress is due to internal pressure which is symmetric about both axes. The applied moments were analyzed by using appropriate symmetric, anti-symmetric or free boundary conditions to represent the full structure of the sweepolet. The stress values presented herein are the highest values at the crack locations.

Based on Reference 4, the applied moments are:

Weight + Seismic = 176,000 inch-pounds

Weight + Steady State Thermal = 246,000 inch-pounds

The maximum primary stress intensity in the sweepolet is 16,600 psi which is significantly less than the allowable of 25,200 psi.

5.4.2 Fracture Mechanics Evaluation

Three types of fracture mechanics evaluations were performed. The allowable crack depth was calculated based on Reference 2. Crack growth due to both fatigue and IGSCC was calculated using the NUTECH computer program NUTCRAK (Reference 8) with material constants and methodology from References 9 and 10. Finally, the ultimate margin to failure for a crack of the depth equal to the upper bound predicted depth after an eighteen month fuel cycle was calculated per References 11 and 12.

5.4.2.1 Allowable Crack Depth

Due to the three-dimensional state of stress that exists at the sweepolet, the allowable depth was calculated in the same manner as for a circumferential crack.

$$\text{Stress Ratio} = \frac{P_m + P_b}{S_m}$$

$$P_m + P_b = 16,600 \text{ psi (Section 5.4.1)}$$

$$S_m = 16,800 \text{ psi}$$

$$\text{Stress Ratio} = 0.99$$

The nondimensional crack length was calculated in the following manner:

$$\frac{l}{t} = \frac{l_f}{(rt)^{1/2}}$$

$$l_f = .50 \text{ inch}$$

$$r = 11.0 \text{ inches}$$

$$t = .975 \text{ inch}$$

Thus per Table IWB-3641-1 (Reference 2) the allowable crack depth is 75 percent of the wall thickness.

5.4.2.2 Crack Growth

The existing cracks could grow due to both fatigue and stress corrosion. Fatigue growth due to the three types of thermal transients defined in Section 4.2 was

calculated using the material properties from Reference 9. The fatigue crack growth for five years of the cycles shown in Figure 5.3 was calculated to be less than 0.01 inch.

IGSCC crack growth was calculated using the upper bound crack growth law shown in Figure 5.5. The residual stress distribution normal to the crack is unknown. It was judged that the sweepolet weld residual stress would be equal or less than that due to a butt weld. Therefore, the residual stress was conservatively assumed to be 30 ksi through-wall bending with tension on the inside surface. The normal stress perpendicular to the crack was determined from the finite element model.

The crack growth analysis was performed per Appendix A of Reference 5. All of the observed cracks are oriented transverse to the sweepolet-to-manifold weld. Therefore, the IGSCC crack length is limited to the width of the heat-affected zone. A finite sized flaw of constant length equal to 1/2 inch was assumed. The predicted crack depth as a function of time is shown in Figure 5.18. Maximum crack depth after 5 years is predicted to be 0.38 inch (38 percent of wall

thickness), which is well below the allowable of 75 percent of wall thickness.

5.4.2.3 Tearing Modulus

The largest size to which the existing sweepolet crack could reasonably be expected to grow to within one fuel cycle was postulated to be a 0.50 inch radius flaw. This assumes growth of the crack at a faster rate than the upper bound prediction in Section 5.4.2.2. A tearing modulus evaluation was then performed for this postulated crack. The applied loads were pressure, seismic, steady state thermal and weight.

The evaluation was performed using the methodology of Reference 11 with material properties from Reference 12.

The postulated flaw and the results are shown in Figure 5.19. The upper dotted line represents the inherent material resistance to unstable fracture in terms of J-integral and Tearing Modulus, T. The line originating at the origin represents the applied loading.

Increasing load results in applied J-T combinations moving up this line, and unstable fracture is predicted

at the intersection of this applied loading line with the material resistance line.

Figure 5.19 shows that the predicted failure load is in excess of 3.3 times the normal operating loads. Thus, there is a safety factor on normal operating loads of at least 3.3, which is well in excess of the safety factor inherent in the ASME Code, even in the presence of this worst case assumed crack.

5.5 Effect on Recirculation and RHR Systems

Installation of the weld overlay repairs caused a small amount of radial and axial shrinkage underneath the overlay. Based on measurements of the weld overlays, the maximum axial shrinkage was 1/4 inch (elbow-to-pipe).

The effects of the radial shrinkage are limited to the region adjacent to and underneath the overlay. Based on Reference 13, the stresses due to the radial shrinkage are less than yield stress at distances greater than 4 inches from the ends of the overlay. Weld residual stresses are steady state secondary stresses and thus are not limited by the ASME Code (Reference 1).

The effect of the axial weld shrinkage on the Recirculation and RHR Systems was evaluated with the NUTECH computer program PISTAR (Reference 14) and the piping model shown in Figure 5.20.

The four end cap weld overlays are adjacent to free ends of the recirculation manifold. Thus, axial weld shrinkage will not induce stress in any other section of the piping. The measured axial shrinkage of the elbow weld overlay (.25 inch) and of the pipe-to-pipe weld overlay (.19 inch) were imposed as boundary conditions on this model. Since the ASME Code does not limit weld residual stress, all stress indices were set equal to 1.0.

The maximum calculated stress was less than 9 ksi. The location of this stress is shown on Figure 5.20. Steady state secondary stresses of 9 ksi are judged to have no deleterious effect on the Recirculation or RHR Systems.

PARAMETER	NORMAL STARTUP CYCLE (CYCLE 1)	SMALL TEMPERATURE CHANGE CYCLE (CYCLE 2)	EMERGENCY CYCLE (CYCLE 3)
EQUIVALENT LINEAR TEMPERATURE ΔT_1	2 ⁰ F	32 ⁰ F	265 ⁰ F
PEAK TEMPERATURE ΔT_2	0	8 ⁰ F	64 ⁰ F
THROUGH WALL THERMAL STRESS σ	368 PSI	8,840 PSI	72,370 PSI

Table 5.1
THERMAL STRESS RESULTS

CATEGORY	EQUATION NUMBER	ACTUAL STRESS OR THICKNESS	SECTION III NB ALLOWABLE
S	N/A	N/A	$S_m = 16,800$ PSI
PRIMARY	(9)	10,590 PSI	25,200 PSI
PRIMARY + SECONDARY	(10)	18,950 PSI	50,400 PSI
PEAK CYCLE 1 CYCLE 2 CYCLE 3	(11)	(23,370)5* (16,950)5 (129,300)5	N/A
USAGE FACTOR (5 YR)	N/A	0.02	1.0

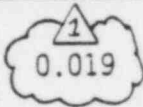
* THE FACTOR OF 5 IS THE CONSERVATIVELY ASSUMED FATIGUE STRENGTH REDUCTION FACTOR.

Table 5.2
END CAP CODE STRESS RESULTS

CATEGORY	EQUATION NUMBER	ACTUAL STRESS OR THICKNESS	SECTION III NB ALLOWABLE
S	N/A	N/A	$S_m = 16,800$ PSI
PRIMARY	(9)	16,200 PSI	25,200 PSI
PRIMARY + SECONDARY	(10)	19,600 PSI	50,400 PSI
PEAK CYCLE 1 CYCLE 2 CYCLE 3	(11)	(16,200)5* (8,800)5 (83,900)5	N/A
USAGE FACTOR (5 YR)	N/A	0.01	1.0

* THE FACTOR OF 5 IS THE CONSERVATIVELY ASSUMED FATIGUE STRENGTH REDUCTION FACTOR.

Table 5.3
ELBOW CODE STRESS RESULTS

CATEGORY	EQUATION NUMBER	ACTUAL STRESS OR THICKNESS	SECTION III NB ALLOWABLE
S	N/A	N/A	$S_m = 16,800$ PSI
PRIMARY	(9)	12,300 PSI	25,200 PSI
PRIMARY + SECONDARY	(10)	16,000 PSI	50,400 PSI
PEAK CYCLE 1 CYCLE 2 CYCLE 3	(11)	(19,500)5* (12,950)5 (125,400)5	N/A
USAGE FACTOR (5 YR)	N/A	 0.019	1.0

* THE FACTOR OF 5 IS THE CONSERVATIVELY ASSUMED FATIGUE STRENGTH REDUCTION FACTOR.

Table 5.4
PIPE-TO-PIPE CODE STRESS RESULTS

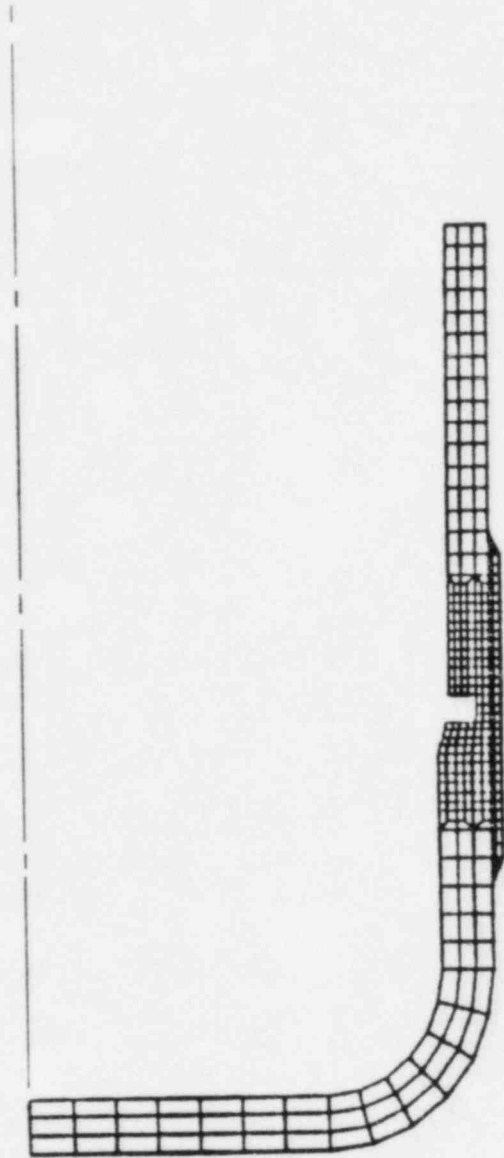
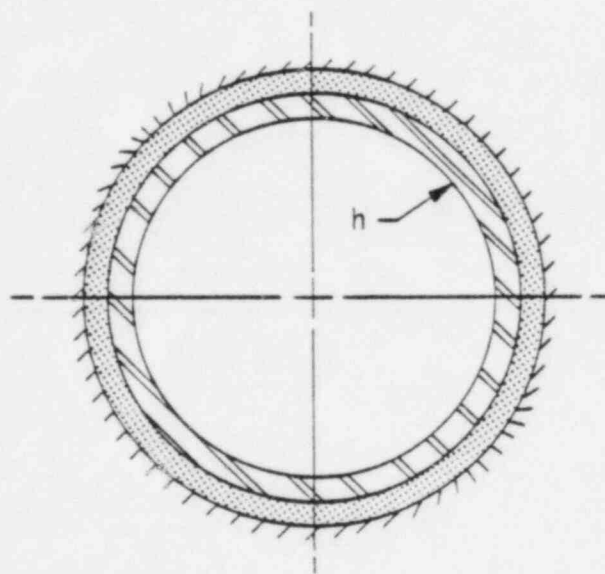
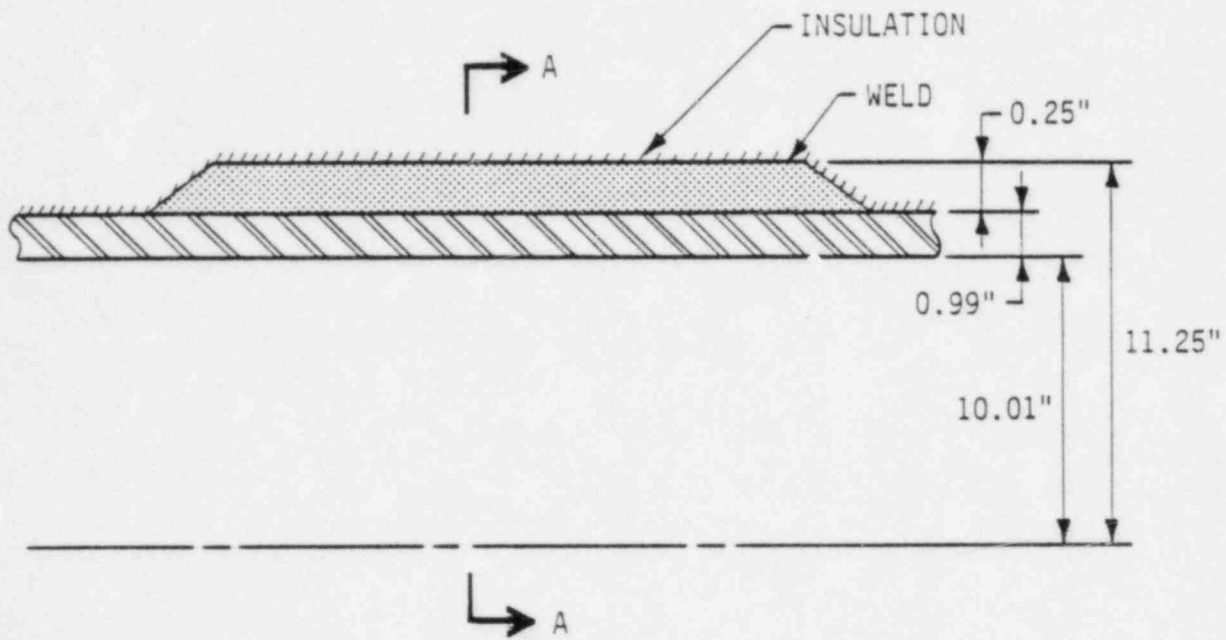


Figure 5.1
END CAP FINITE ELEMENT MODEL



SECTION A-A

$h = \infty$
 $k = 10 \text{ BTU/hr-ft-}^{\circ}\text{F}$

Figure 5.2
 WELD OVERLAY THERMAL MODEL

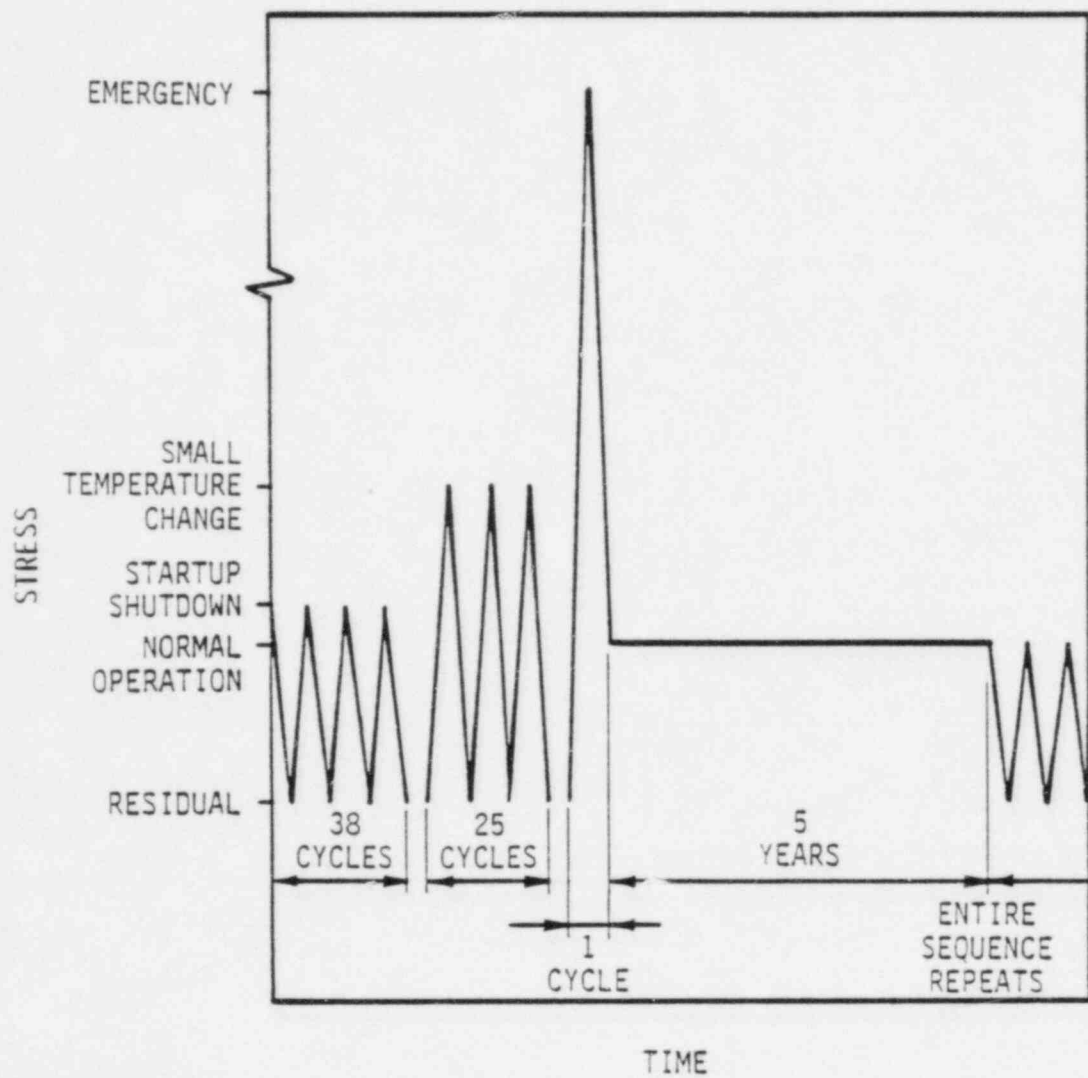


Figure 5.3
THERMAL TRANSIENTS

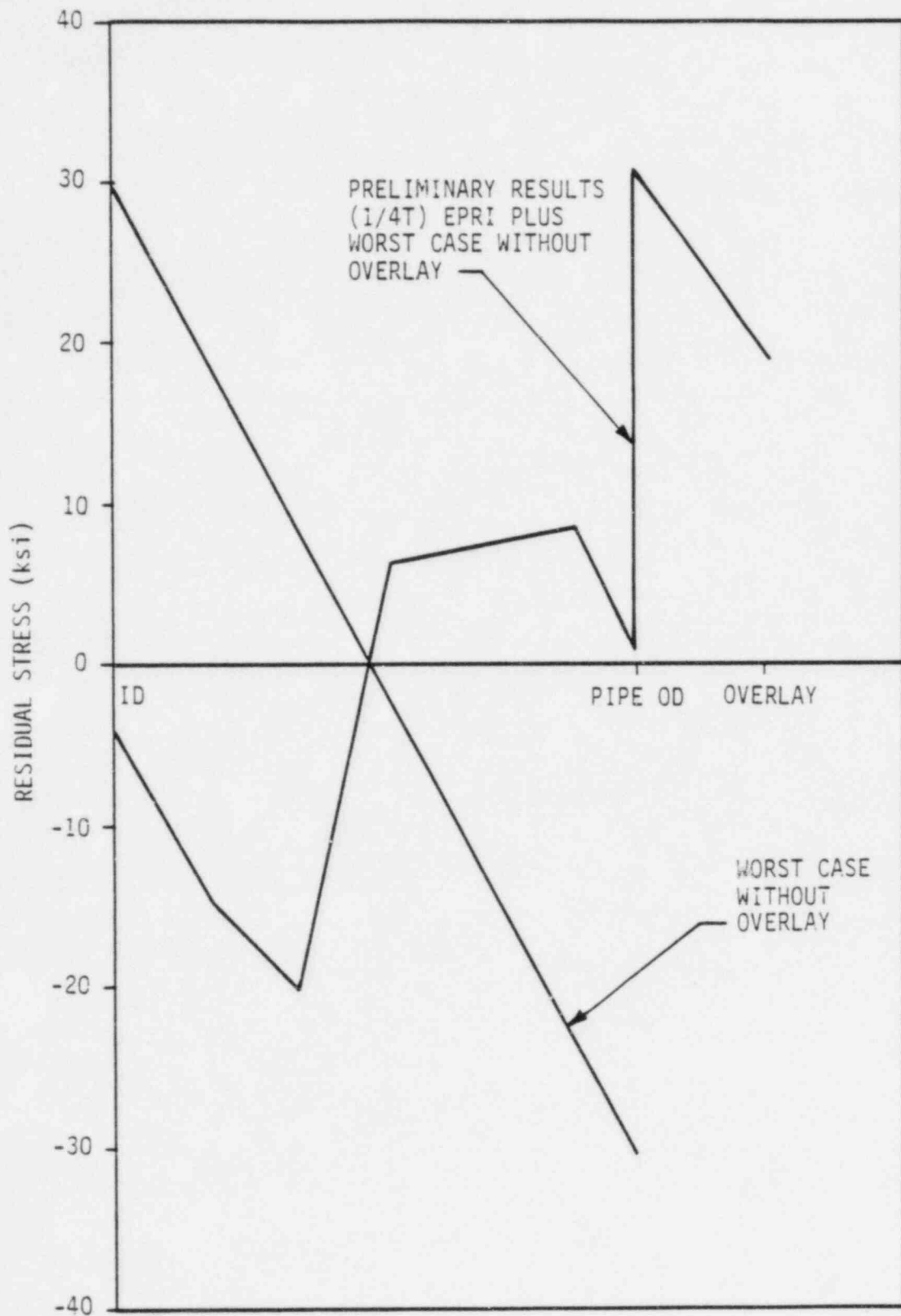


Figure 5.4
AXIAL CRACK GROWTH RESIDUAL STRESS

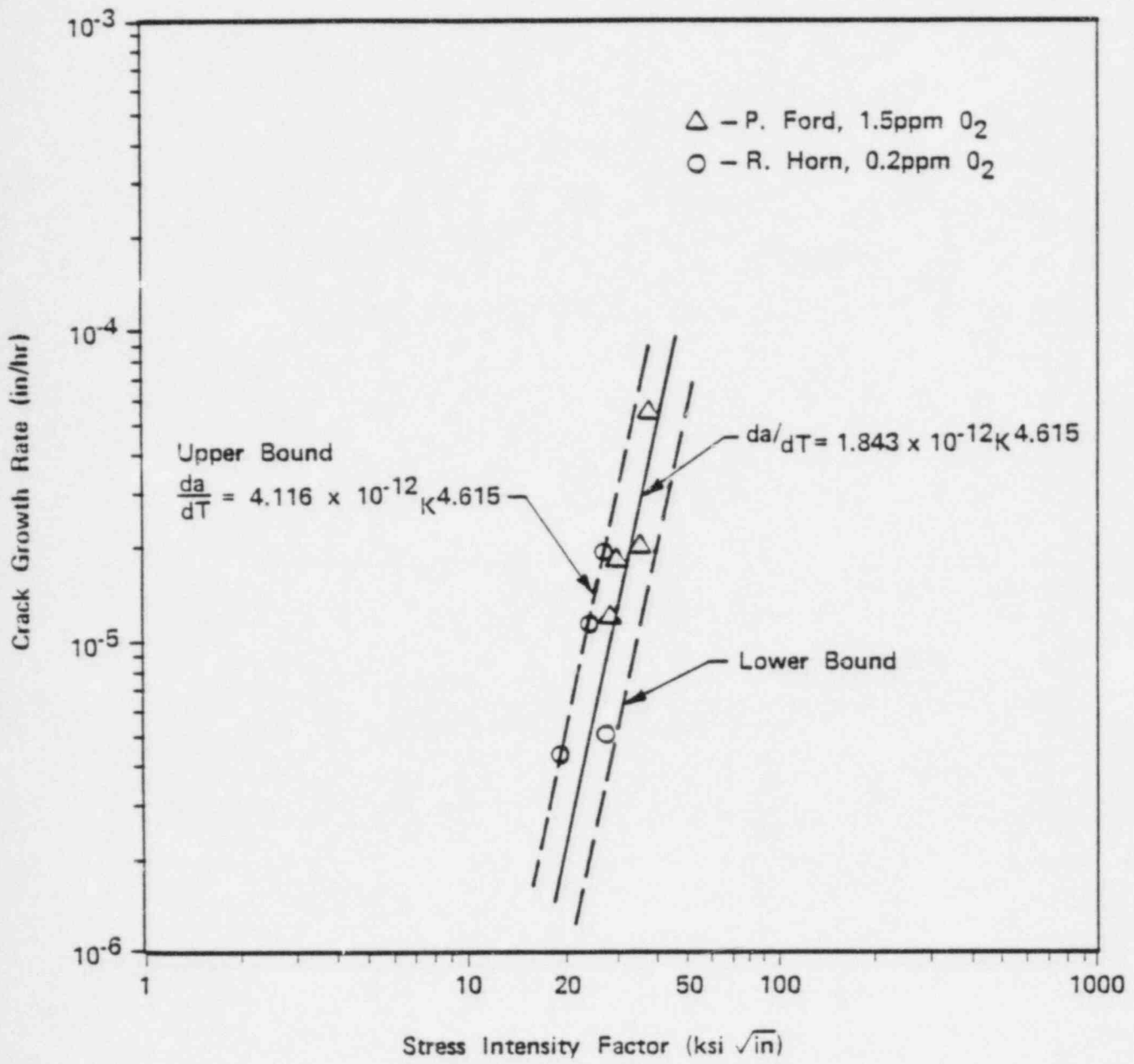


Figure 5.5
 TYPICAL IGSCC CRACK GROWTH DATA
 (WELD SENSITIZED 304SS IN BWR ENVIRONMENT)

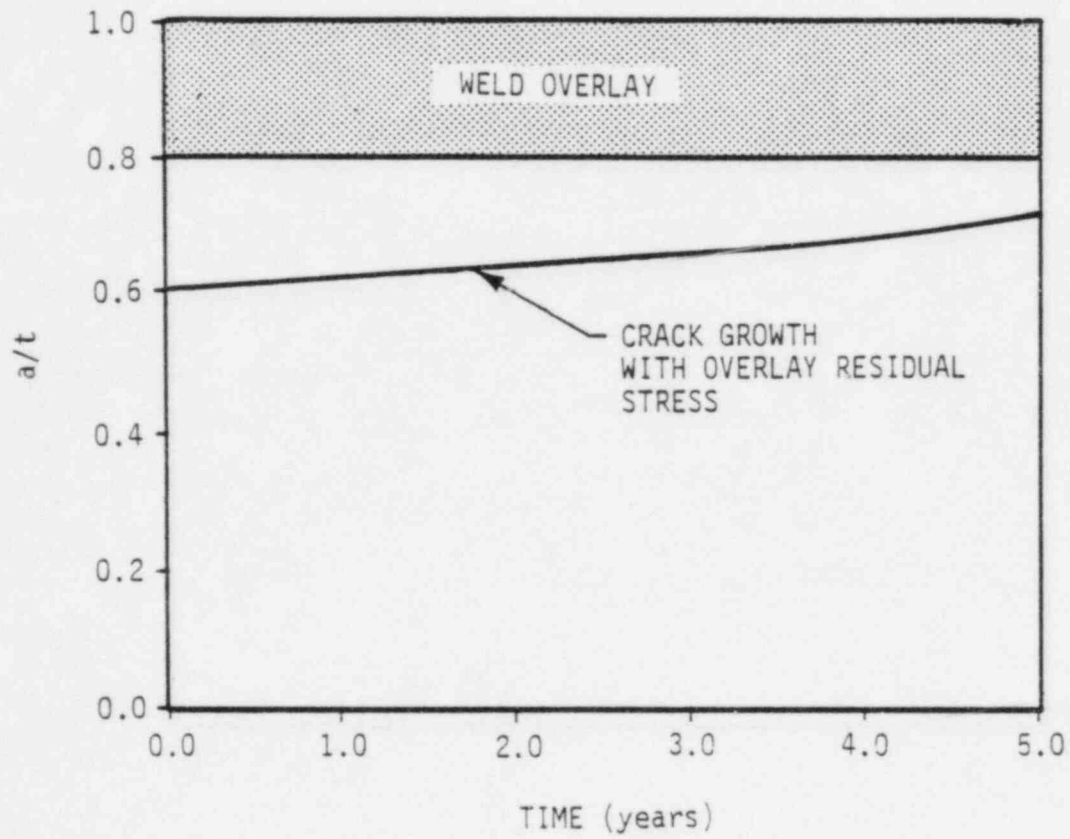
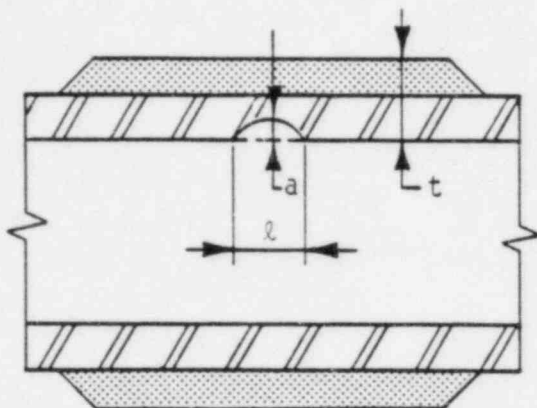


Figure 5.6
END CAP AXIAL CRACK GROWTH

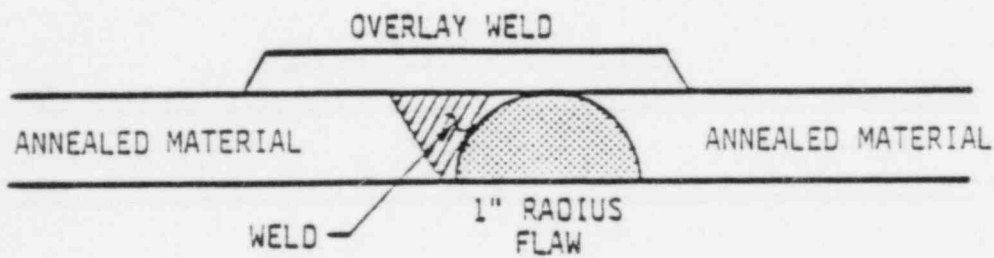
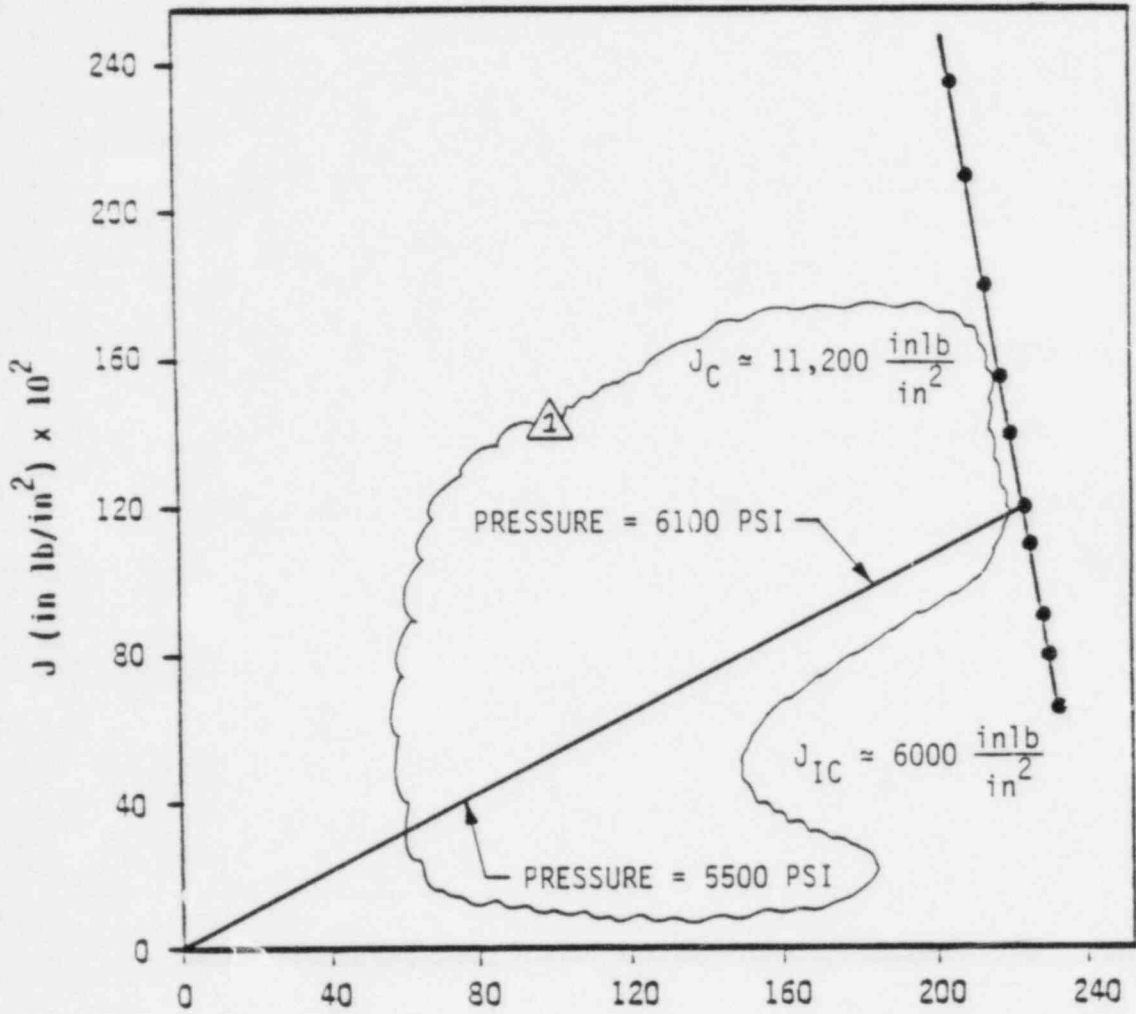
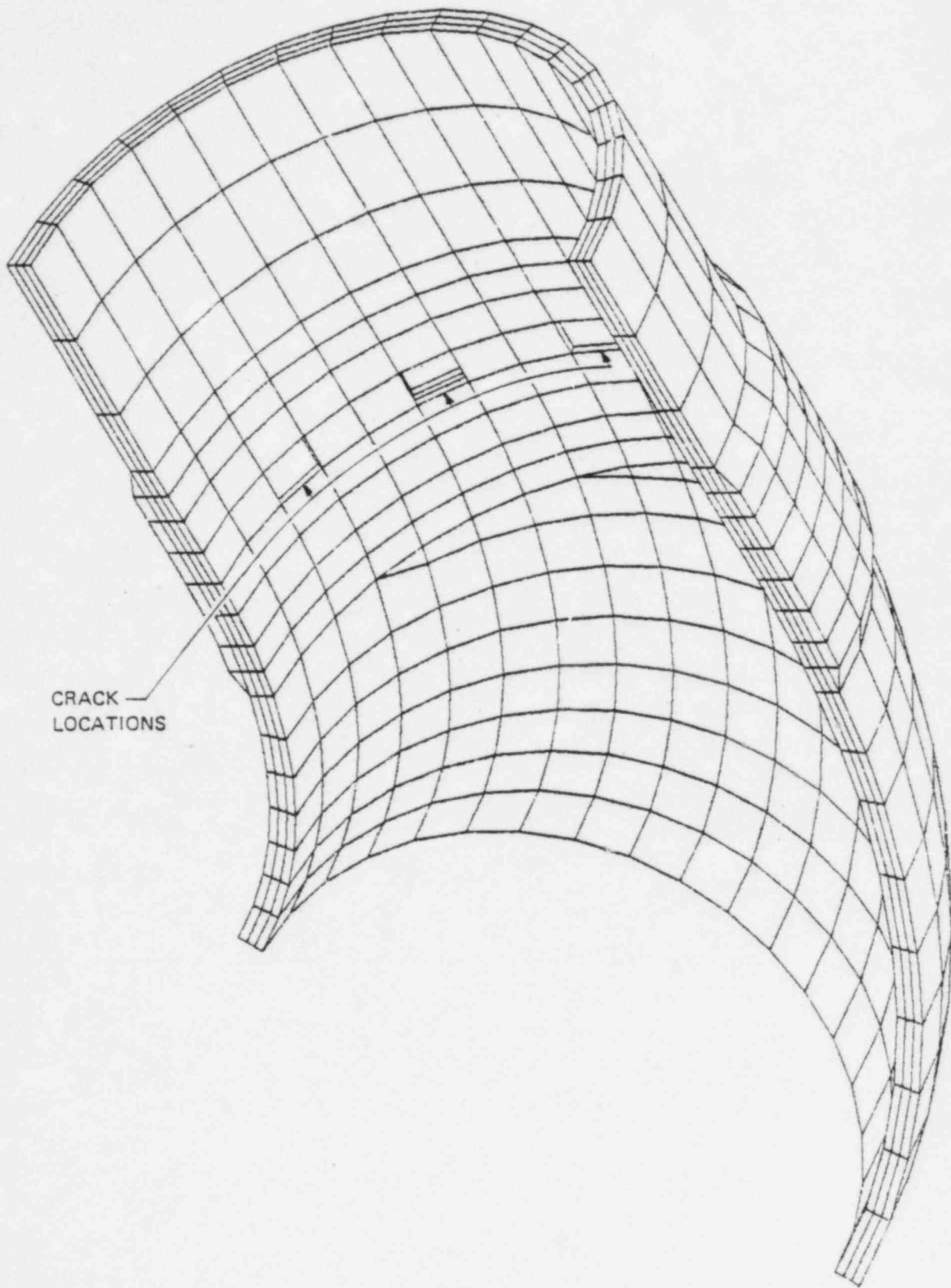


Figure 5.7
END CAP TEARING MODULUS



CRACK —
LOCATIONS

Figure 5.8
ELBOW FINITE ELEMENT MODEL

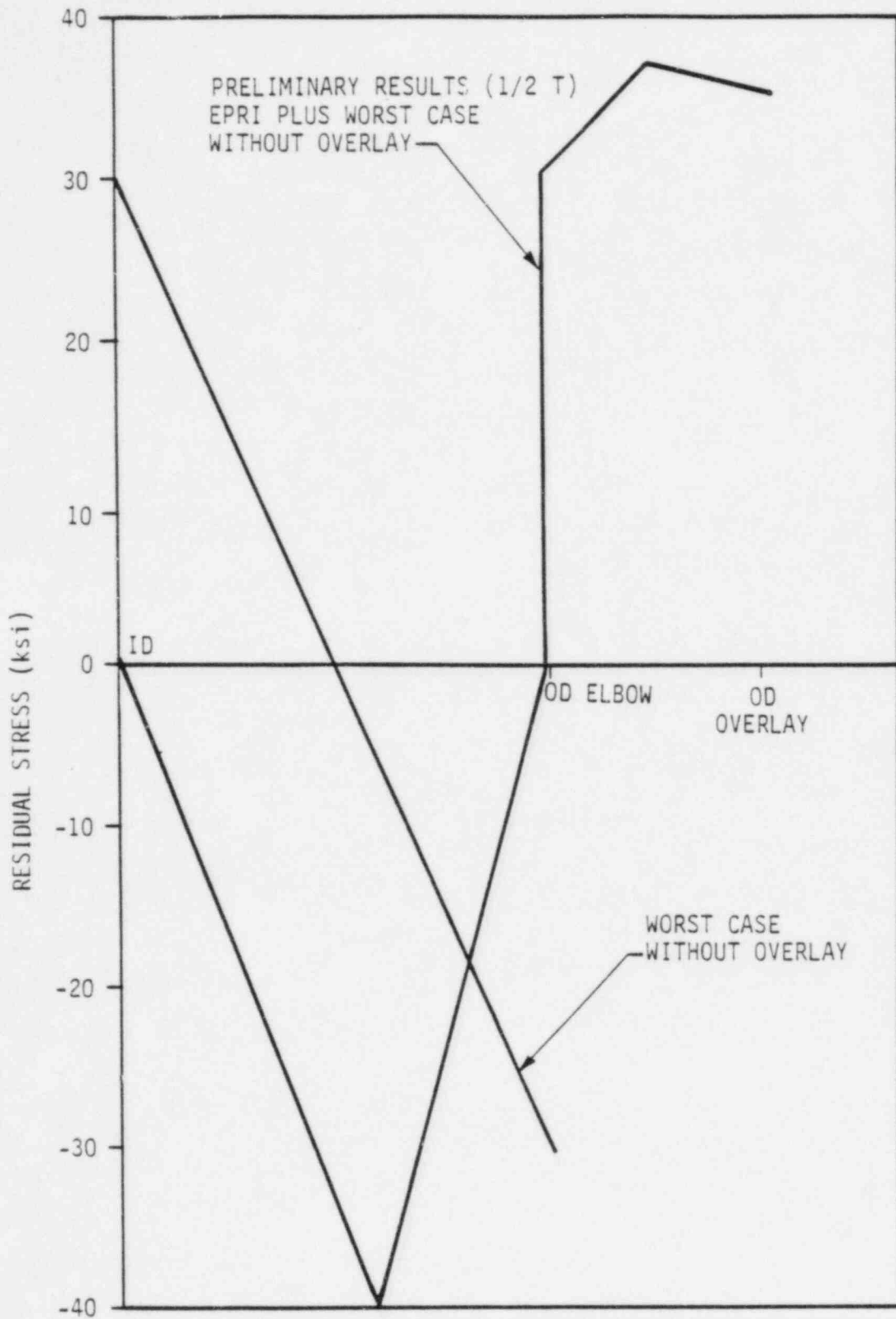


Figure 5.9
CIRCUMFERENTIAL CRACK GROWTH RESIDUAL STRESS

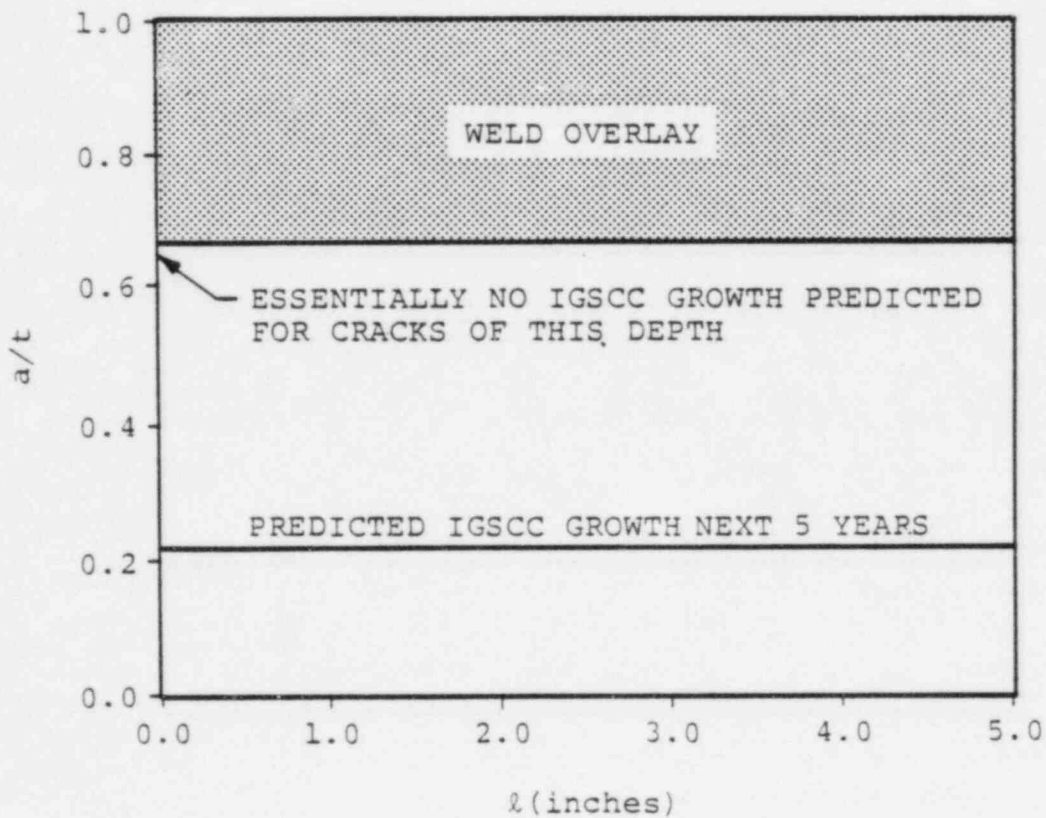
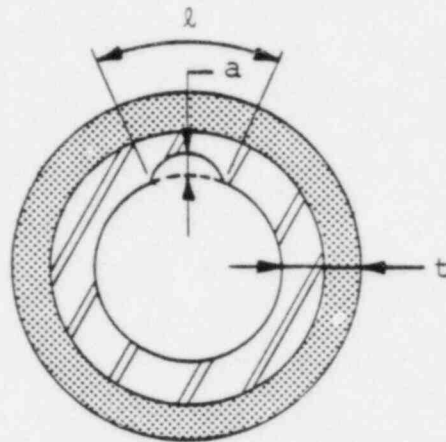


Figure 5.10
ELBOW CIRCUMFERENTIAL CRACK GROWTH

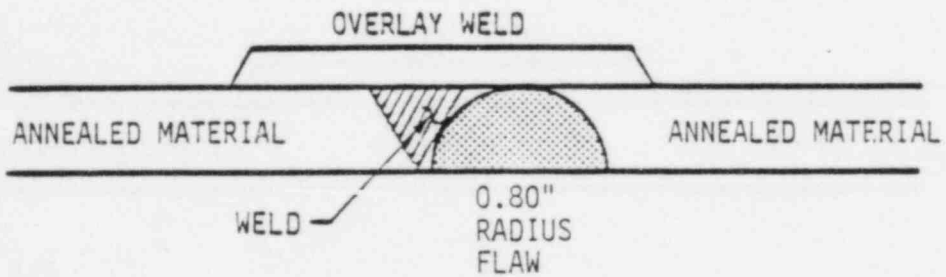
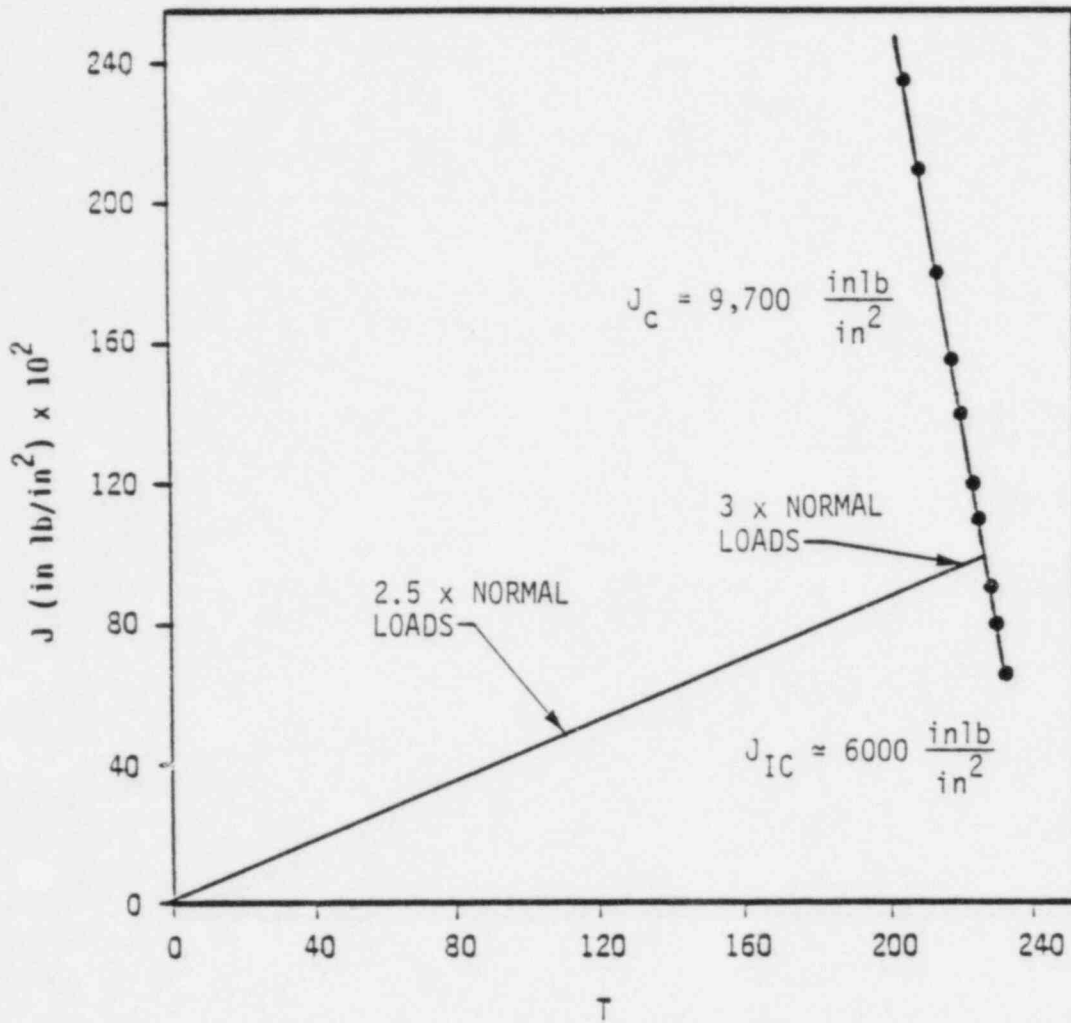


Figure 5.11
ELBOW TEARING MODULUS

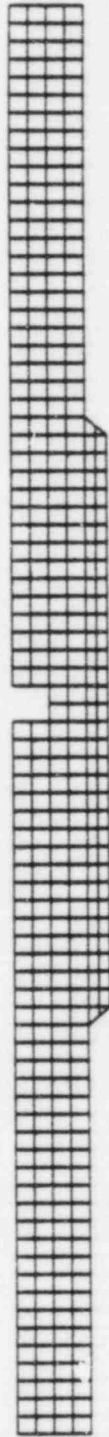


Figure 5.12
PIPE-TO-PIPE FINITE ELEMENT MODEL

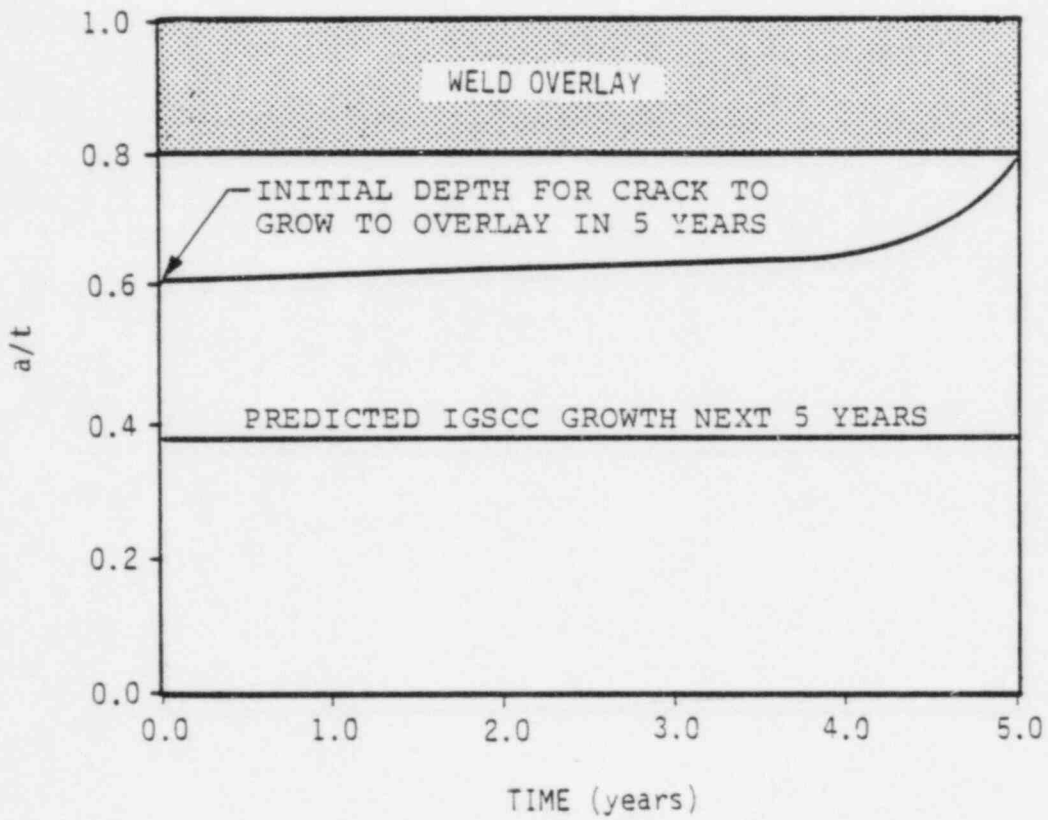
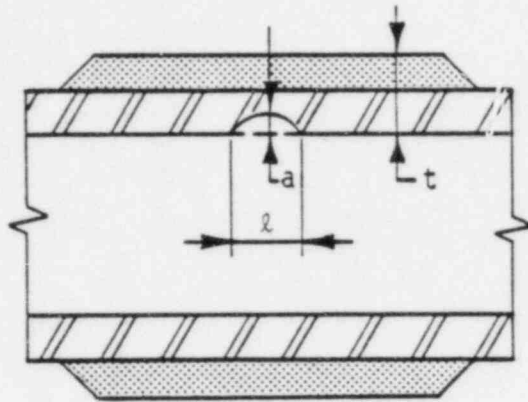


Figure 5.13
PIPE-TO-PIPE AXIAL CRACK GROWTH

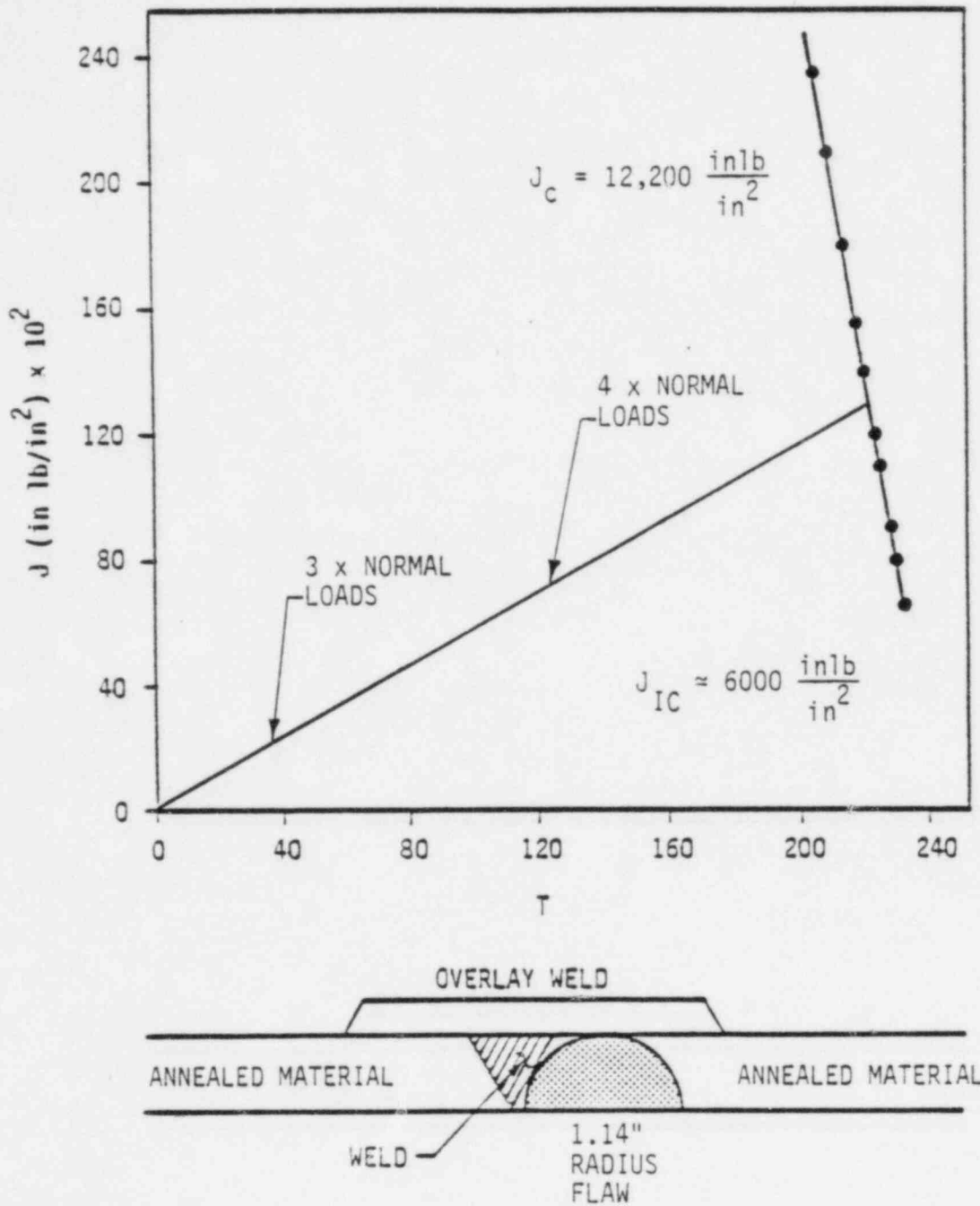
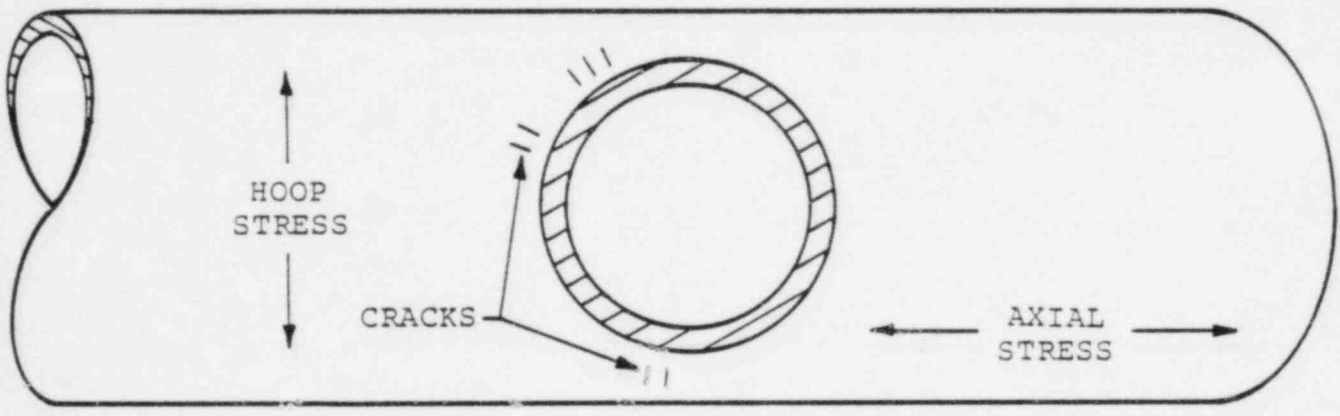
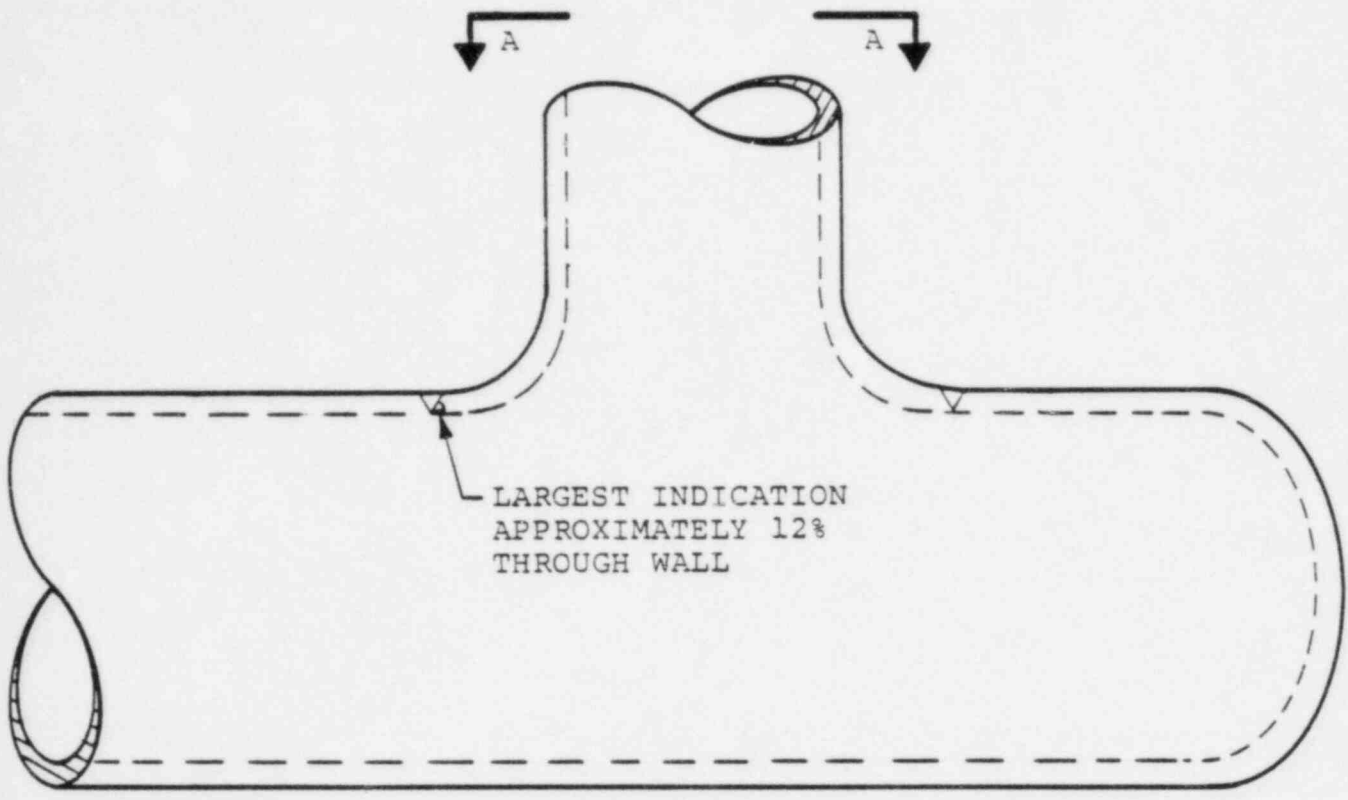


Figure 5.14
PIPE-TO-PIPE TEARING MODULUS



VIEW A-A

Figure 5.15
SWEEPOLET CRACK GEOMETRY

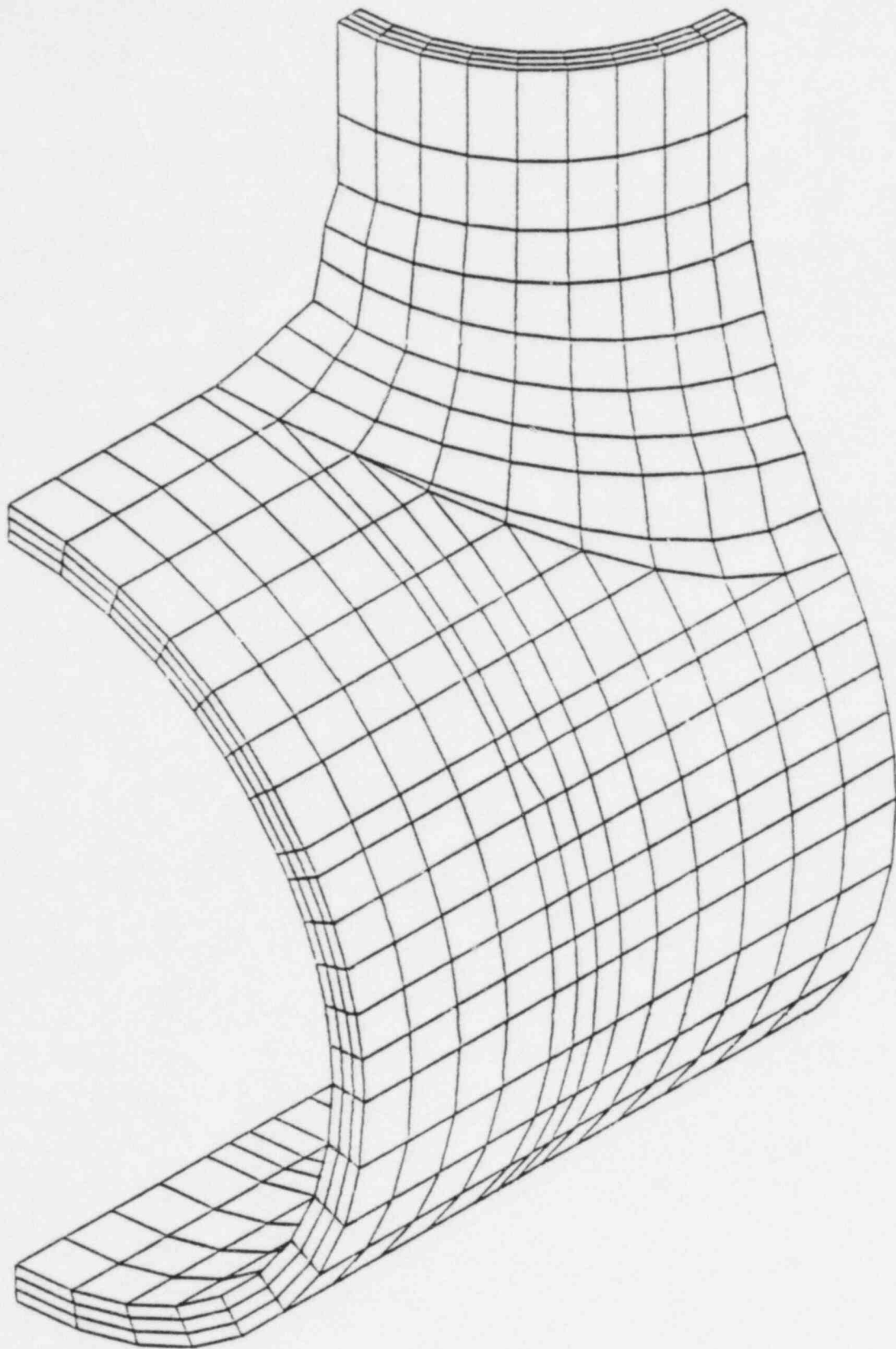


Figure 5.16
SWEEPOLET FINITE ELEMENT MODEL (OUTSIDE)

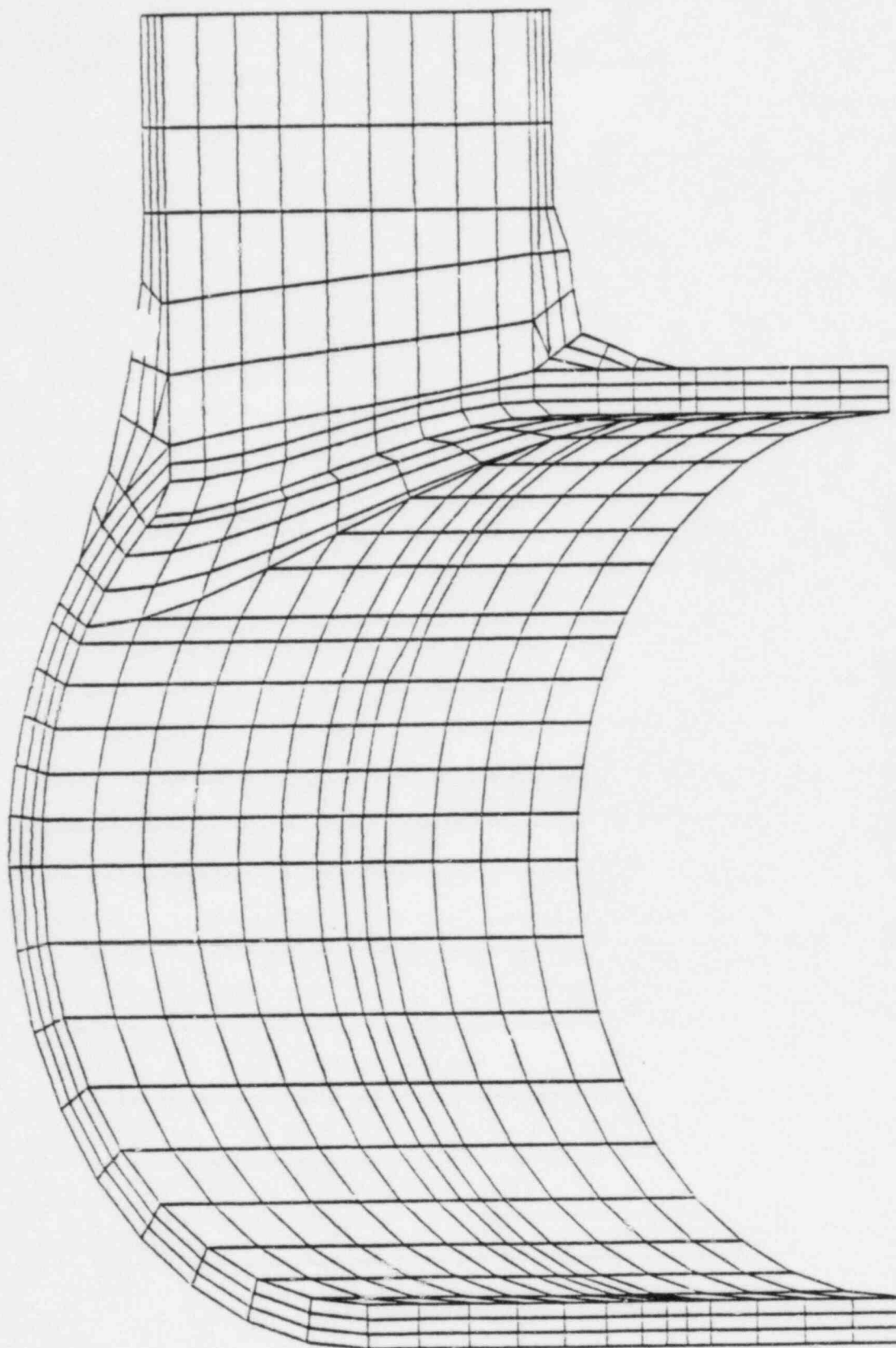


Figure 5.17
SWEEPOLET FINITE ELEMENT MODEL (INSIDE)

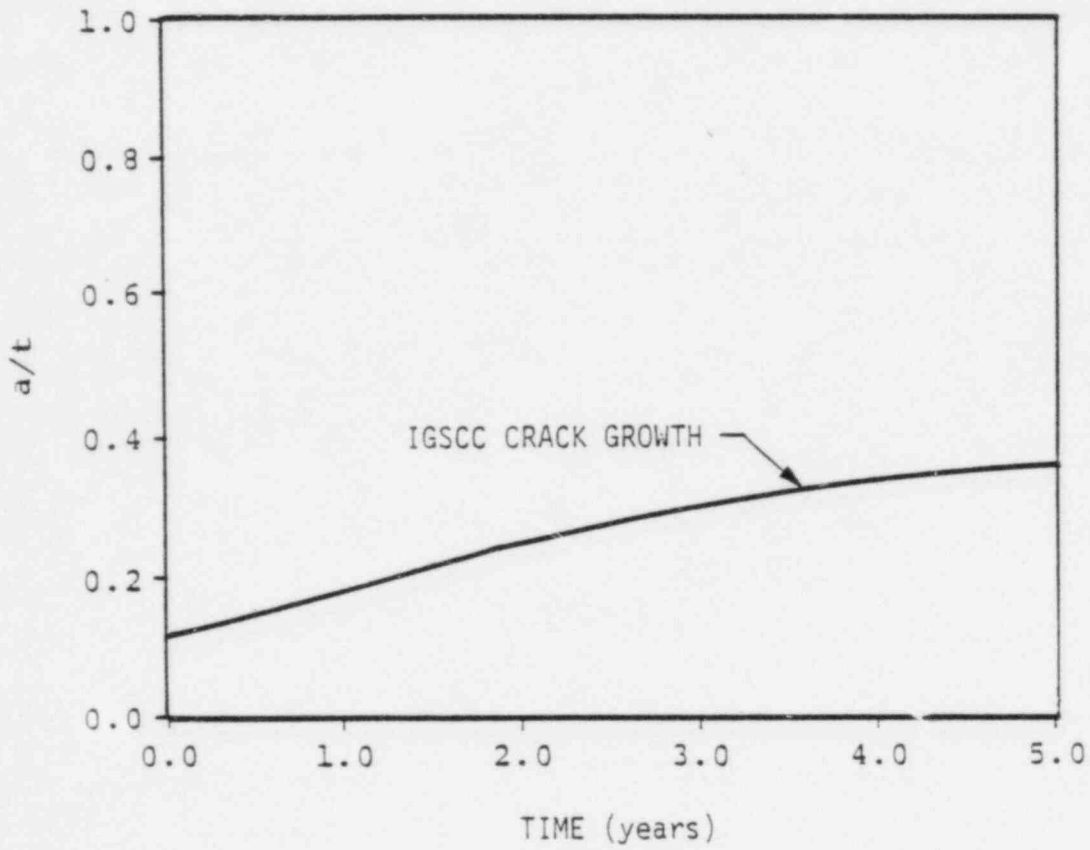
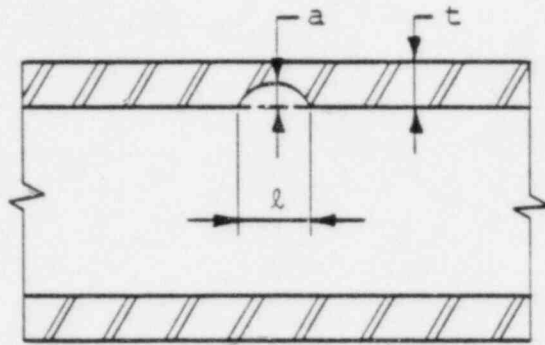


Figure 5.18
SWEEPOLET CRACK GROWTH

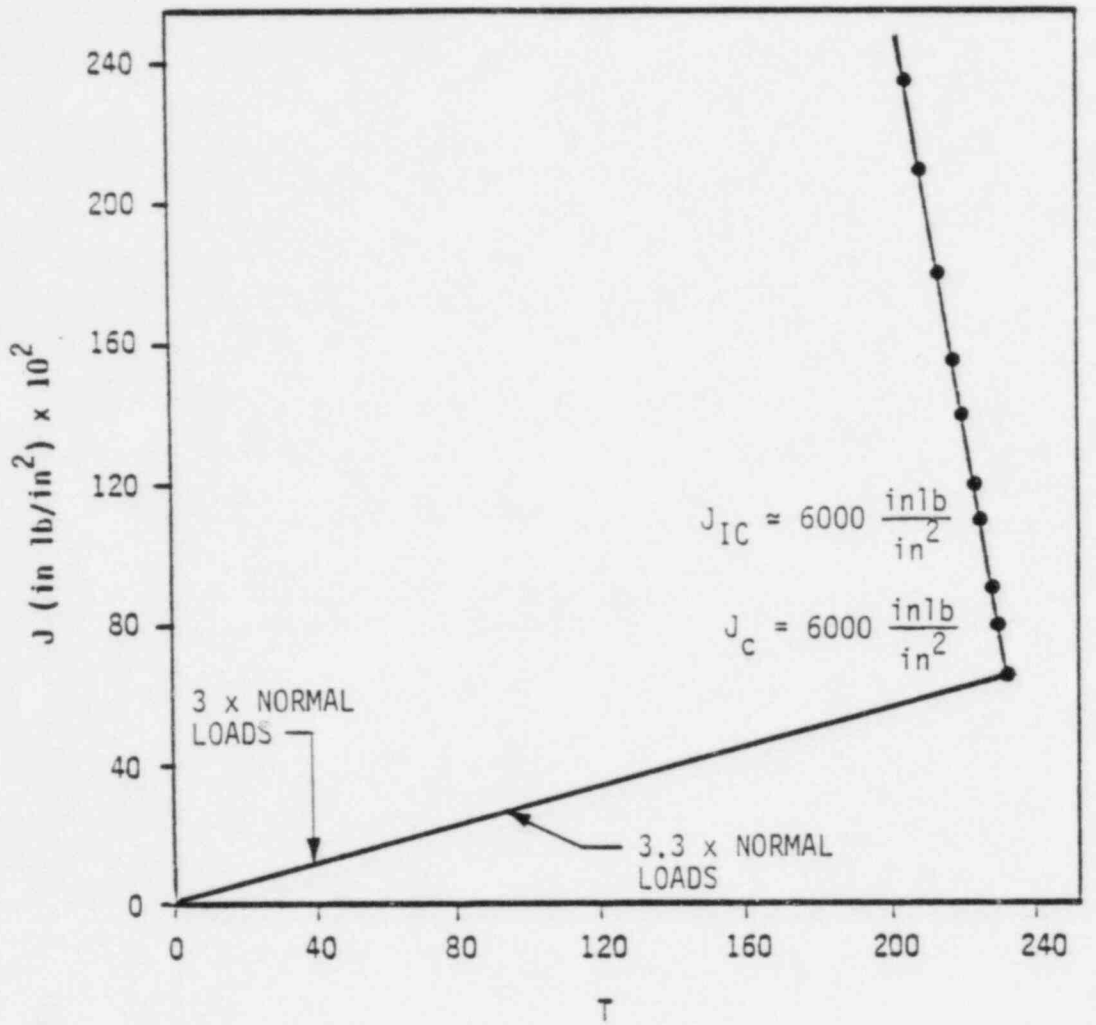


Figure 5.19
SWEEPOLET TEARING MODULUS

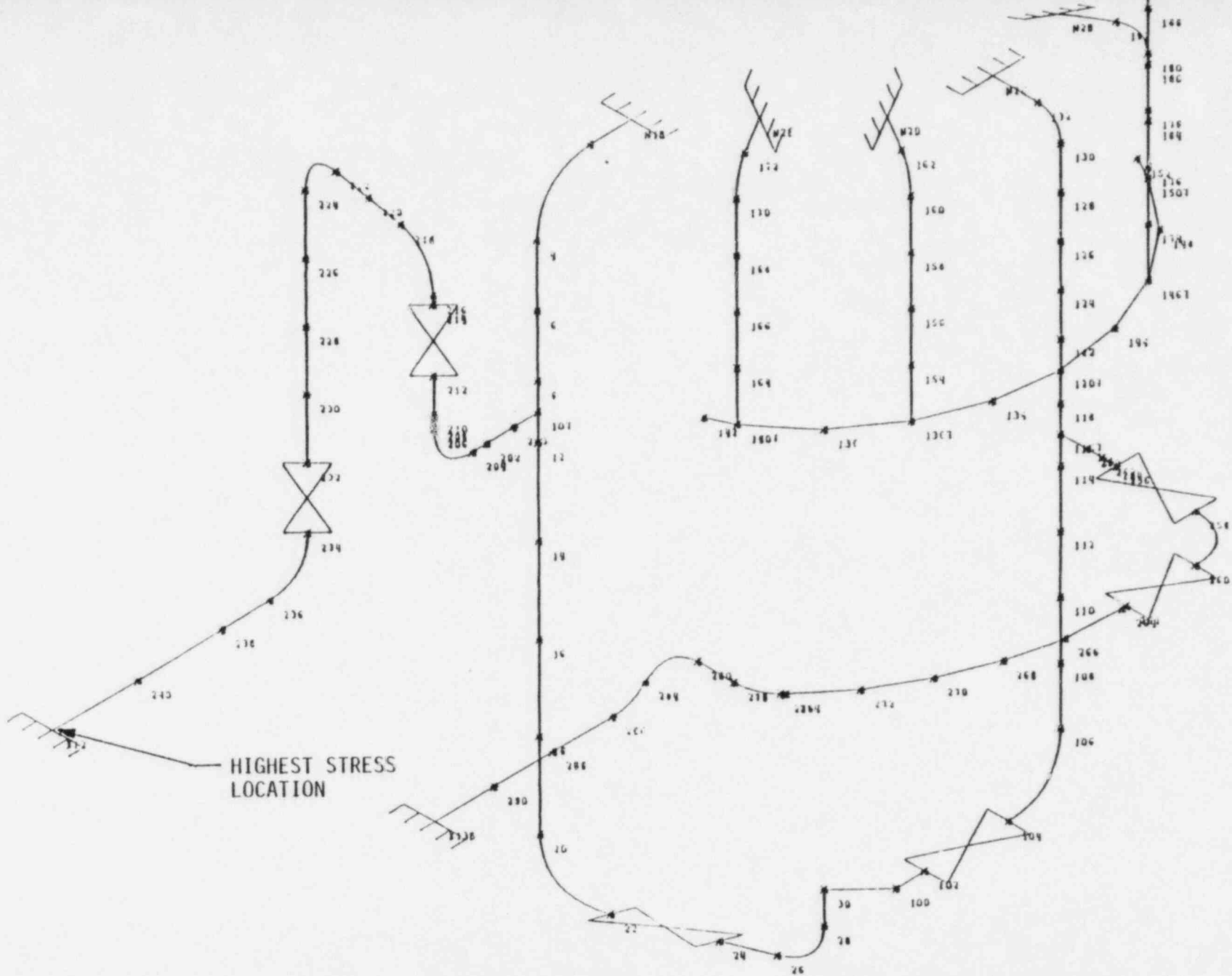


Figure 5.20
PIPING MODEL

6.0 LEAK-BEFORE-BREAK

6.1 Net Section Collapse

The simplest way to determine the effect of IGSCC on the structural integrity of piping is through the use of a simple "strength of materials" approach to assess the load carrying capacity of a piping section after the cracked portion has been removed. Studies have shown (References 10 and 12) that this approach gives a conservative, lower-bound estimate of the loads which would cause unstable fracture of the cracked section. Typical results of such an analysis are indicated in Figure 6.1 (Reference 10). This figure defines the locus of limiting crack depths and lengths for circumferential cracks which are predicted to cause failure by the net section collapse method. Curves are presented for both typical piping system stresses and stress levels equal to ASME Code limits. Note that a very large percentage of pipe wall can be cracked before reaching these limits (40% to 60% of circumference for through-wall cracks, and 65% to 85% of wall thickness for 360° part-through cracks).

Also shown in Figure 6.1 is a sampling of cracks which have been detected in service, either through UT examination or leakage. In each case there has been a comfortable margin between the size crack that was observed and that which would be predicted to cause failure under service loading conditions. Also, as discussed below, there is still considerable margin between these net section collapse limits and the actual cracks which would cause instability.

6.2 Tearing Modulus Analysis

Elastic-plastic fracture mechanics analyses are presented in Reference 12 which give a more accurate representation of the crack tolerance capacity of stainless steel piping than the net section collapse approach described above. Figures 6.2 and 6.3 graphically depict the results of such an analysis (Reference 12). Through-wall circumferential defects of arc-length equal to 60° through 300° were assumed at various cross sections of a typical BWR Recirculation System. Loads were applied to these sections of sufficient magnitude to produce net section limit load, and the resulting values of tearing modulus were compared to that required to cause unstable fracture

(Figure 6.2). Note that in all cases there is substantial margin, indicating that the net section collapse limits of the previous section are not really failure limits. Figure 6.3 summarizes the results of all such analyses performed for 60° through-wall cracks in terms of margin on tearing modulus for stability. The margin in all cases is substantial.

6.3

Leak Versus Break Flaw Configuration

Of perhaps more significance to the leak-before-break argument is the flaw configuration depicted in Figure 6.4. This configuration addresses the concerns raised by the occurrence of part-through flaws growing, with respect to the pipe circumference, before breaking through the outside surface to cause leakage. Figure 6.4 presents typical size limitations on such flaws based on the conservative, net section collapse method of Section 6.1. Note that very large crack sizes are predicted. Also shown on this figure are typical detectability limits for short through-wall flaws (which are amenable to leak detection) and long part-through flaws (which are amenable to detection by UT). The margins between the detectability limits, and the conservative, net section collapse failure limits are

substantial. It is noteworthy that the likelihood of flaws developing which are characterized by the vertical axis shown in Figure 6.4 (full 360° circumferential with no through-wall component) is so remote as to be considered impossible. Material and stress asymmetries always tend to propagate one portion of the crack faster than the bulk of the crack front, which will eventually result in "leak-before-break". This observation is borne out by extensive field experience with BWR IGSCC.

6.4 Axial Cracks

The recent IGSCC occurrences at Monticello and Hatch 1 were predominately short, axial cracks which grew through the wall but remained very short in the axial direction. This behavior is consistent with expectations for axial IGSCC since the presence of a sensitized weld heat-affected zone is necessary, and this heat-affected zone is limited to approximately 0.25 inch on either side of the weld. Since the major loadings in the above net section collapse analysis are bending moments on the cross section due to seismic loadings, and since these loads do not exist in the circumferential direction, the above leak-before-break arguments are even more persuasive for axially oriented

cracks. There is no known mechanism for axial cracks to lengthen before growing through-wall and leaking, and the potential rupture loading on axial cracks is less than that on circumferential cracks.

6.5 Multiple Cracks

Recent analyses performed for EPRI (Reference 15) indicate that the occurrence of multiple cracks in a weld, or cracking in multiple welds in a single piping line do not invalidate the leak-before-break arguments discussed above.

6.6 Crack Detection Capability

IGSCC in BWR piping is detected through two means: non-destructive examination (NDE) and leakage detection. Although neither is perfect, the two means complement one another well. This detection capability combined with the exceptional inherent toughness of stainless steel, results in essentially 100% probability that IGSCC would be detected before it significantly degraded the structural integrity of a BWR piping system.

The primary means of nondestructive examination for IGSCC in BWR piping is ultrasonics (UT). This method has been the subject of considerable research and development in recent years, and significant improvements in its ability to detect IGSCC have been achieved. Nevertheless, recent UT experience at Monticello, Hatch 1, and elsewhere indicate that there is still considerable room for improvement, especially in the ability to distinguish cracks or crack-like indications from innocuous geometric conditions.

Figure 6.4, however, illustrates a significant aspect of UT detection capability with respect to leak-before-break. The types of cracking most likely to go undetected by UT are relatively short circumferential or axial cracks which are most amenable to detection by leakage. Conversely, as part-through cracks lengthen, and thus become more of a concern with respect to leak-before-break, they become readily detectable by UT, and are less likely to be misinterpreted as geometric conditions. This argument is further enhanced by the usual practice of supplementing the UT inspection with radiography (RT) when large UT indications are

observed. If a long UT indication is truly a geometric condition, it will be observable as density differences on the radiograph. If, on the other hand, no significant RT density differences are observed in the vicinity of the UT indication, (or if the density differences are abrupt and crack-like), the observed indication is usually diagnosed as IGSCC.

6.8 Leakage Detection

Typical leakage detection capability for BWR reactor coolant system piping is through sump level and drywell activity monitoring. These systems have sensitivities on the order of 1.0 gallon per minute (GPM) of unidentified leakage (i.e., not from known sources such as valve packing or pump seals). Plant technical specification limits typically require investigation/corrective action at 5.0 GPM unidentified leakage.

Table 6.1 provides a tabulation of typical flaw sizes to cause 5.0 GPM leakage in various size piping (Reference 10).

Also shown in this table are the critical crack lengths for through-wall cracks based on the net section

collapse method of analysis discussed above. For conservatism, the leakage values are based on pressure stress only, while the critical crack lengths are based on the sum of all combined loads, including seismic. (Considering other normal operating loads in the leakage analysis would result in higher rates of leakage for a given crack size.) Note that there is considerable margin between the crack length to produce 5.0 GPM leakage and the critical crack length, and that this margin increases with increasing pipe size.

6.9 Historical Experience

The above theories regarding crack detectability have been borne out by experience. Indeed, of the approximately 400 IGSCC incidents to date in BWR piping, all have been detected by either UT or leakage, and none have even come close to violating the structural integrity of the piping (Reference 15).

NOMINAL PIPE SIZE	CRACK LENGTH FOR 5 GPM LEAK (in.)	CRITICAL CRACK LENGTH l_c (in.)	l/l_c
4" SCH 80	4.50	6.54	0.688
10" SCH 80	4.86	15.95	0.305
24" SCH 80	4.97	35.79	0.139

Table 6.1
EFFECT OF PIPE SIZE ON THE RATIO OF THE CRACK LENGTH
FOR 5 GPM LEAK RATE AND THE CRITICAL CRACK LENGTH
(ASSUMED STRESS $\sigma = S_m/2$)

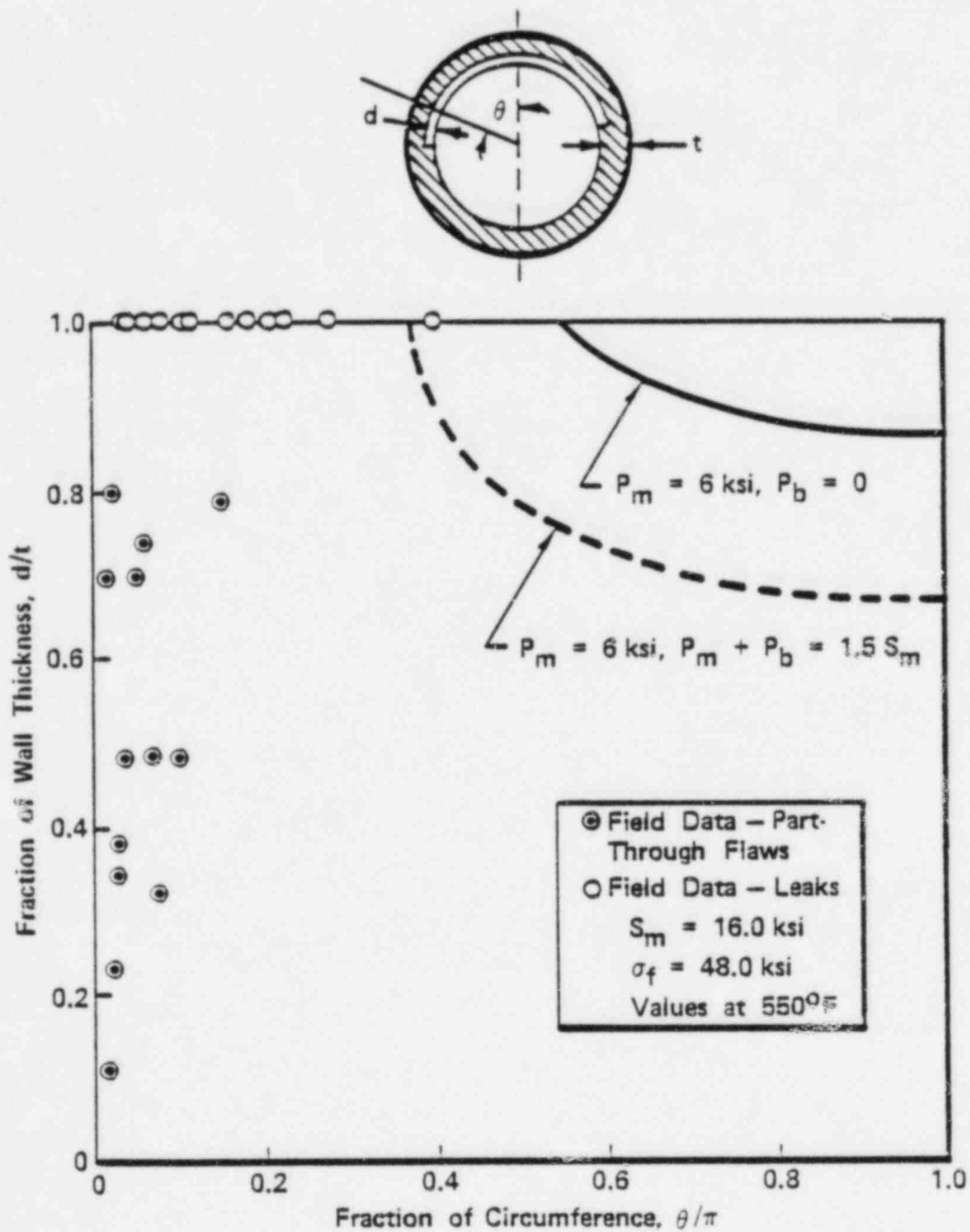


Figure 6.1
TYPICAL RESULT OF NET SECTION COLLAPSE ANALYSIS OF
CRACKED STAINLESS STEEL PIPE

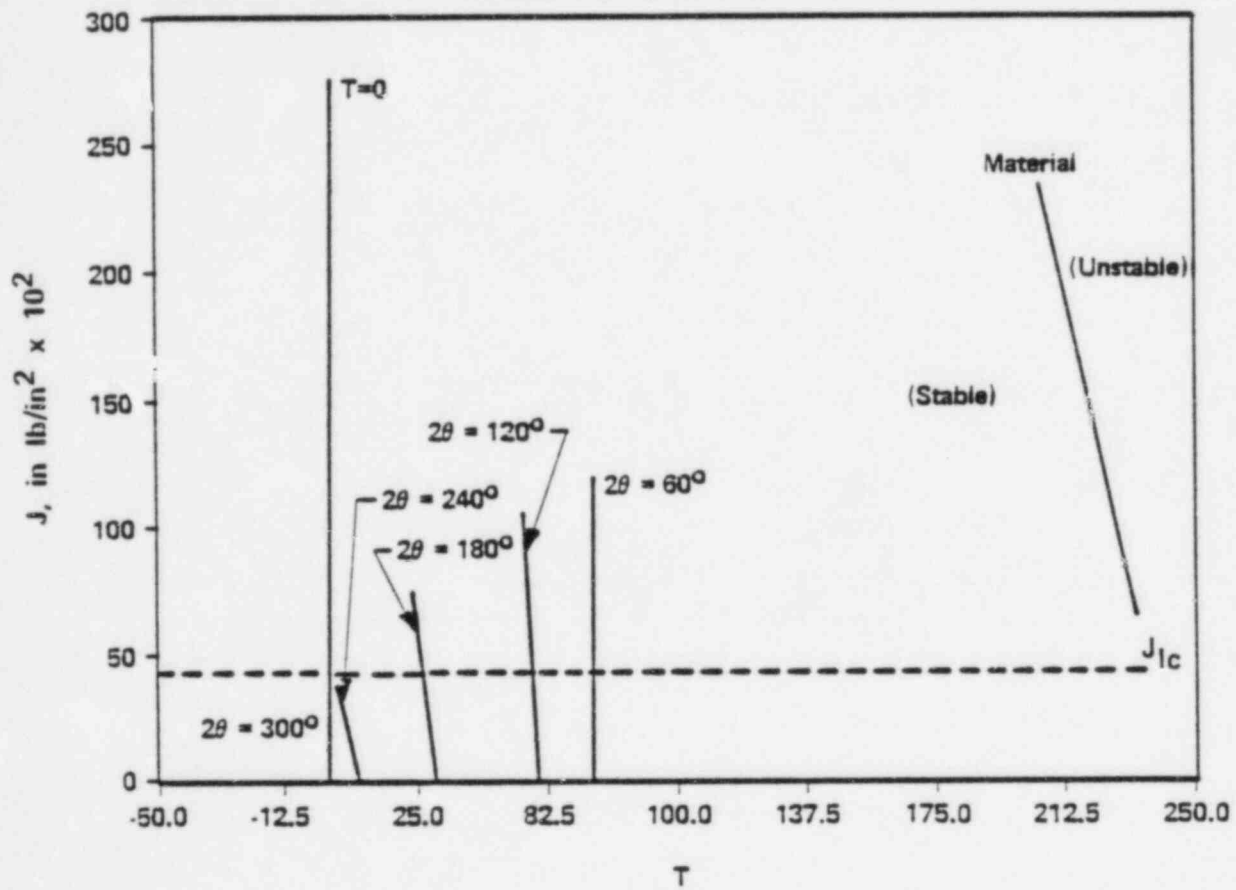
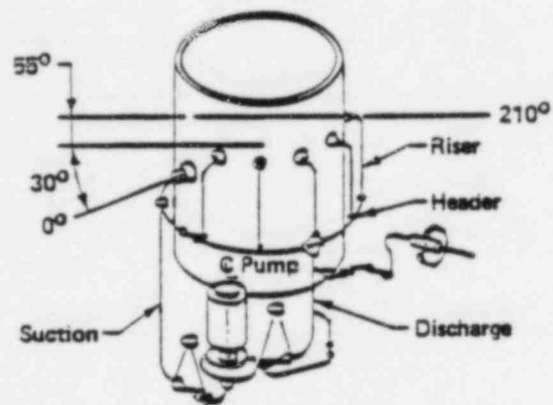


Figure 6.2
 STABILITY ANALYSIS FOR BWR RECIRCULATION SYSTEM
 (STAINLESS STEEL)

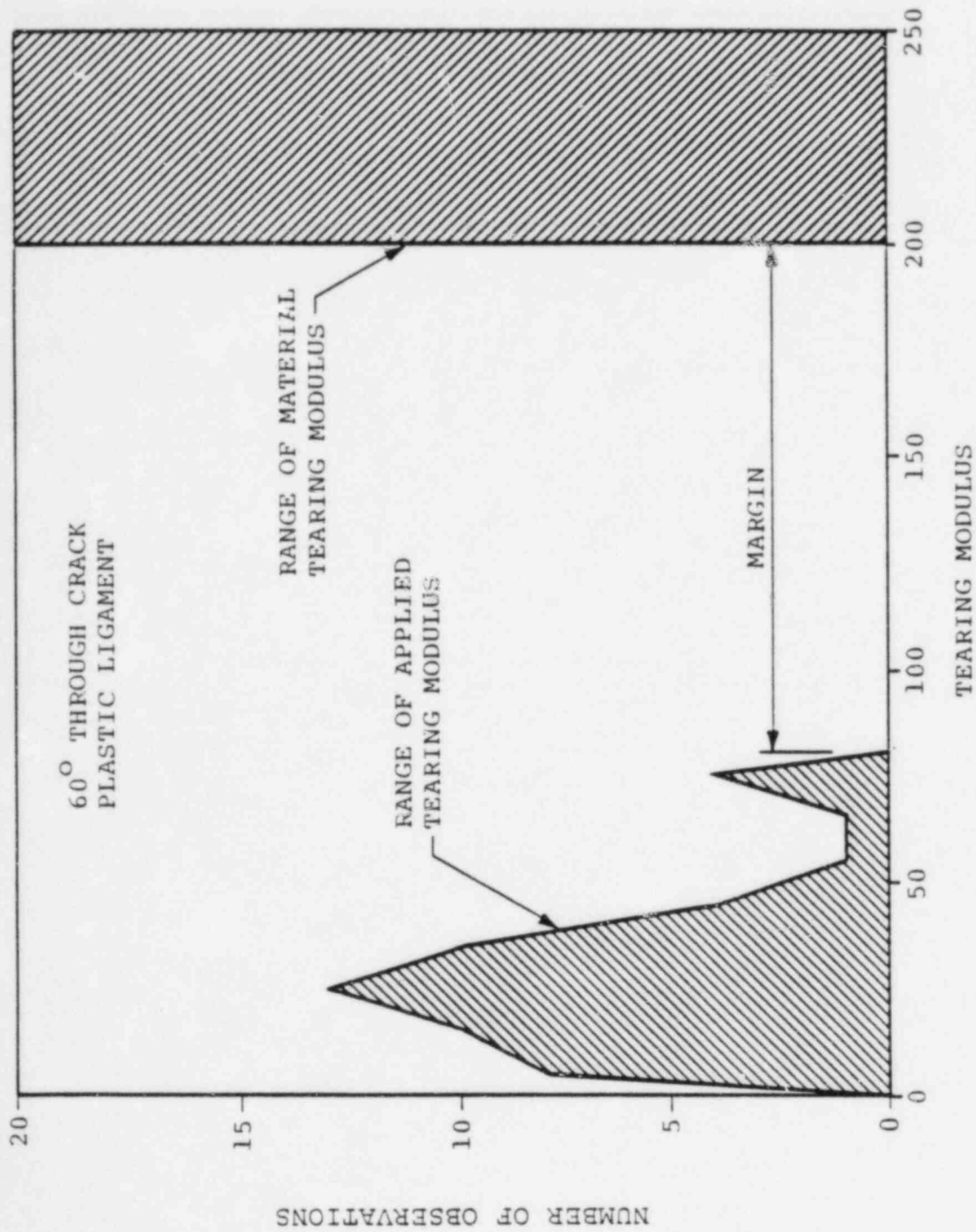
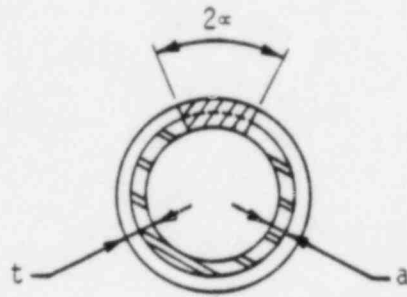


Figure 6.3
SUMMARY OF LEAK BEFORE BREAK ASSESSMENT
OF BWR RECIRCULATION SYSTEM



PIPE CROSS SECTION

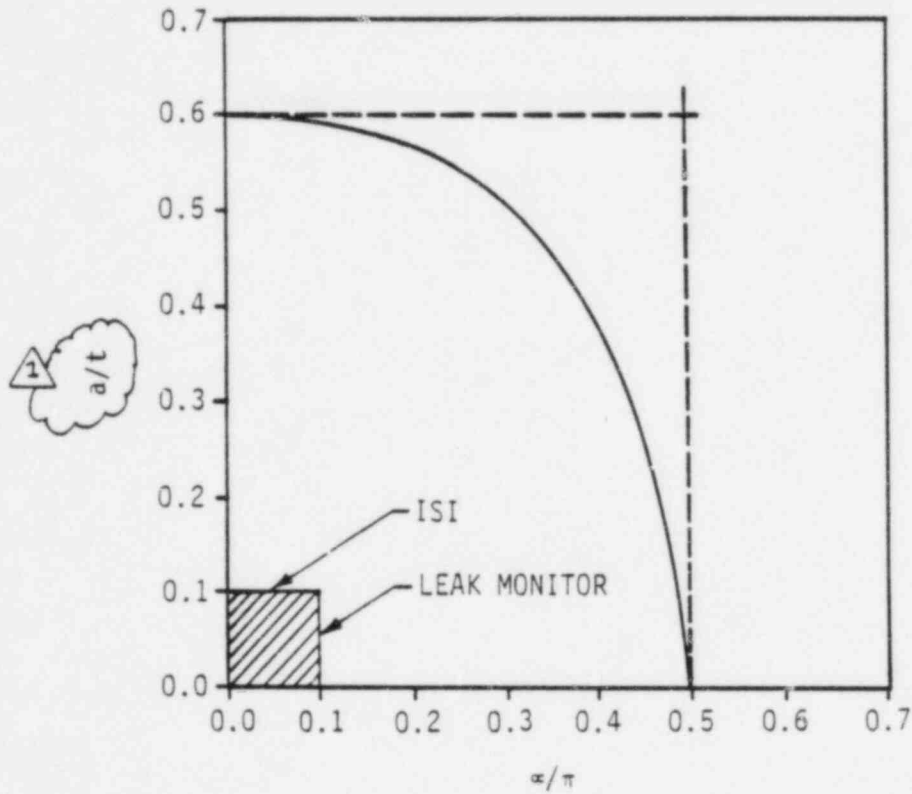


Figure 6.4
TYPICAL PIPE CRACK FAILURE LOCUS FOR COMBINED
THROUGH WALL PLUS 360° PART THROUGH CRACK

The evaluation of the sweepolet flaws and the repairs to the Recirculation and RHR Systems reported herein shows that the resulting stress levels are acceptable for all design conditions. The stress levels have been assessed from the standpoint of load capacity of the components, fatigue, and the resistance to crack growth.

Acceptance criteria for the analyses have been established in Section 3.0 of this report which demonstrate that:

1. There is no loss of design safety margin over that provided by the current Code of Construction for Class 1 piping and pressure vessels (ASME Section III).
2. During the design lifetime of each repair, the observed cracks will not grow to the point where the above safety margins would be exceeded.

Analyses have been performed and results are presented which demonstrate that the sweepolet flaws and the

repaired welds satisfy these criteria by a large margin, and that:

1. The design life of each repair is at least five years.
2. The sweepolet flaws will not grow to an unacceptable size within five years.

Furthermore, it is concluded that the recent IGSCC experienced in the reactor recirculation system at Hatch 1 does not increase the probability of a design basis pipe rupture at the plant. This conclusion expressly considers the nature of the cracking which has been repaired at Hatch 1, and the likelihood that other similar cracking may have gone undetected. The conclusion is based primarily on the extremely high inherent toughness and ductility of the stainless steel piping material; the tendency of cracks in such piping to grow through-wall and leak before affecting its structural load carrying capacity (which indeed was the case in the defects observed at Hatch 1); and the fact that as cracks lengthen and are less likely to "leak-before-break", they become more amenable to detection by other NDE techniques such as UT and RT.

REFERENCES

1. ASME Boiler and Pressure Vessel Code Section III, Subsection NB, 1974 Edition with Addenda through Summer 1975.
2. ASME Boiler and Pressure Vessel Code Section XI, Paragraph IWB-3640 (Proposed), "Acceptance Criteria for Austenitic Stainless Steel Piping" (Presented to Section XI Subgroup on Evaluation Standards in November 1982).
3. General Electric Design Specification 22A1344, Revision 3.
4. General Electric letter G-GPC-2-511, "IE Bulletin 79-14 for E. I. Hatch Nuclear Plant Unit 1 - Transmittal of Preliminary Results of Recirculation System Analysis and Design Drawings," December 17, 1982.
5. ASME Boiler and Pressure Vessel Code Section XI, 1980 Edition with Addenda through Winter 1981.

6. ANSYS Computer Program, Swanson Analysis Systems, Revisions 3 and 4.
7. Schneider, P. J., "Temperature Response Charts," John Wiley and Sons, 1963.
8. NUTCRAK Computer Program, Revision 0, April 1978, File Number 08.039.0005.
9. EPRI-2423-LD, "Stress Corrosion Cracking of Type 304 Stainless Steel in High Purity Water - a Compilation of Crack Growth Rates," June 1982.
10. EPRI-NP-2472, "The Growth and Stability of Stress Corrosion Cracks in Large-Diameter BWR Piping," July 1982.
11. NUREG-0744, Volume 1 for Comment, "Resolution of the Reactor Materials Toughness Safety Issue."
12. EPRI-NP-2261, "Application of Tearing Modulus Stability Concepts to Nuclear Piping," February 1982.

13. NUTECH Report NSP-81-105, Revision 2, "Design Report for Recirculation Line Safe End and Elbow Repair, Monticello Nuclear Generating Plant," December 1982.
14. NUTECH Computer Program PISTAR, Version 2.0, Users Manual, Volume 1, TR-76-002, Revision 4, File Number 08.003.0300.
15. Presentation by EPRI and BWR Owners Group to U.S. Nuclear Regulatory Commission, "Status of BWR IGSCC Development Program," October 15, 1982.

During the installation of the weld overlays, one situation occurred which required an engineering change. The overlay of the pipe-to-pipe weld (1E11-1RHR-24-BR-13) was closer to the pipe to carbon steel valve weld (1E11-1RHR-24-BR-12) than was expected (Figure 9.1). Cracks occurred on the outside surface of the pipe adjacent to the weld overlay (Figure 9.1).

All cracks were removed by grinding to a maximum depth of approximately 0.1 inch. The grinding was extended to approximately the center of the BR-12 weld. The ground out region was then inlaid with NiCrFe weld (Figure 9.2). The weld inlay will produce compressive stresses similar to a weld overlay. Thus the potential for future IGSCC in the stainless steel heat affected zone on the inside of the pipe piece adjacent the BR-12 weld has been significantly reduced by the NiCrFe inlay.

The pipe-to-pipe finite element model was modified to represent the new design (Figure 9.3). The stresses tabulated in Table 5.4 bound the corresponding stresses for the uncracked BR-12 weld.

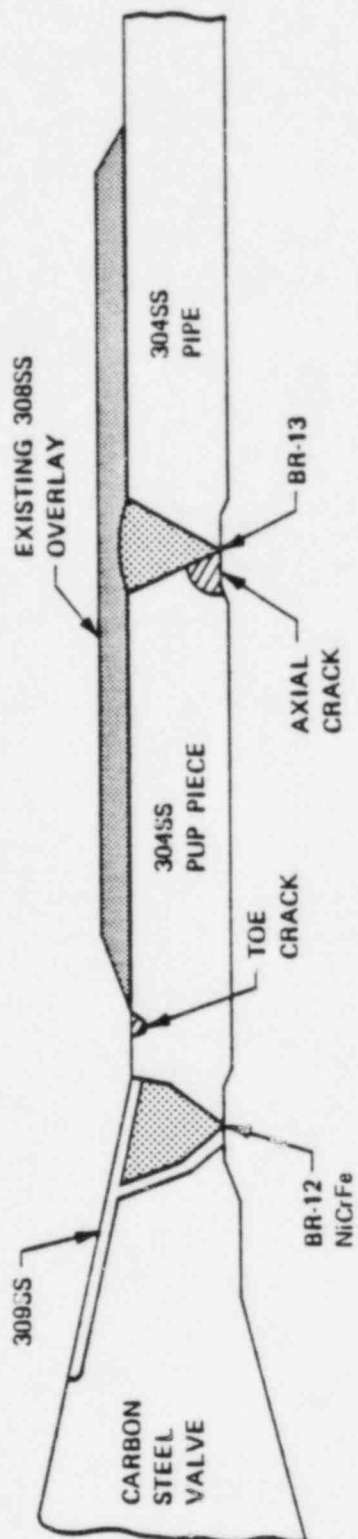


Figure 9.1
 SKETCH OF BR-13 OVERLAY TOE CRACK

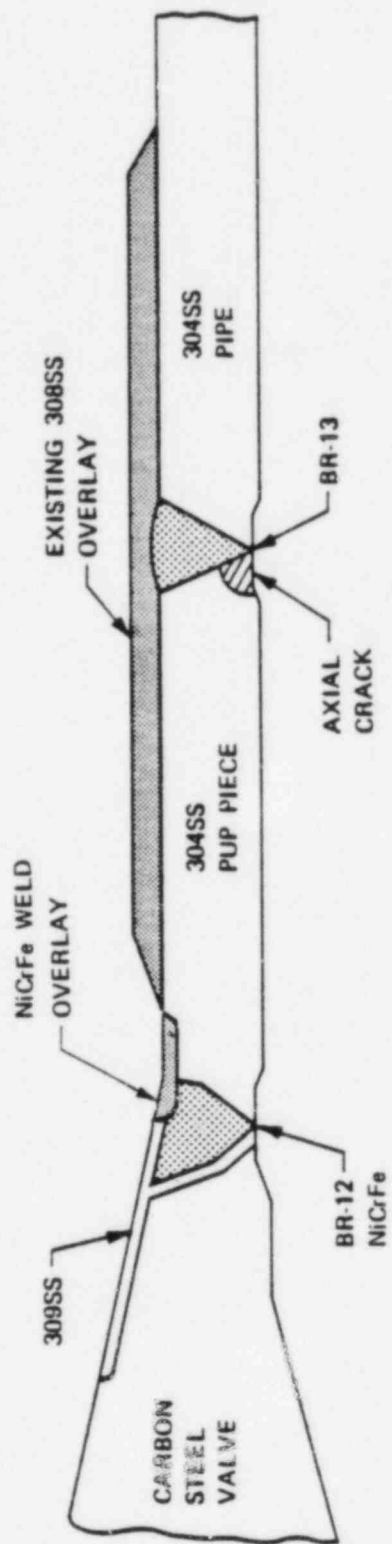


Figure 9.2
 SKETCH OF REVISED BR-13 OVERLAY

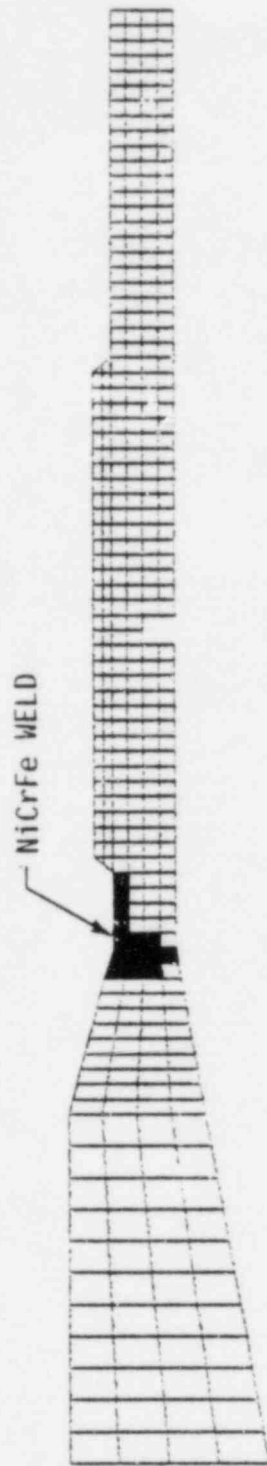


Figure 9.3
REVISED PIPE-TO-PIPE FINITE ELEMENT MODEL